

**Jurassic–Cretaceous deformational phases in the Paraná
intracratonic basin, southern Brazil**

**A. J. Strieder^{1,*}, R. Heemann², P. A. R. Reginato³, R. B. Acauan⁴, V. A. de
Amorim⁵, and M. Z. Remde⁶**

[1] {Engenharia Geológica, Centro de Engenharia, UFPel

Praça Domingos Rodrigues 02, Bairro Porto, Pelotas–RS, Brazil, CEP 96.010-440}

adelirstrieder@uol.com.br

Tel.: +55 51 3921.1419

[2] {PUC-RS, Porto Alegre–RS, Brazil, CEP 90.619-900}

roberto.heemann@pucrs.br

[3] {IPH, UFRGS, Porto Alegre–RS, Brazil, CEP 91.501-970}

pedro.reginato@ufrgs.br

[4] {FEPAM, Porto Alegre–RS, Brazil, CEP 90.020-021}

robby_bonato@yahoo.com.br

[5] {Non-affiliated, Geologist, Professional Services}

nessa_amorim@yahoo.com

[6] {Non-affiliated, Engineering Geologist, Professional Services}

mzremde@gmail.com

Excluído: c

Código de campo alterado

Código de campo alterado

1 [*] {now at: CERENA - Centro de Recursos Naturais e Ambiente
2 Instituto Superior Técnico (Universidade de Lisboa), Av. Rovisco Pais Lisboa 1049-001,
3 Portugal}
4

5 *Correspondence to: A. J. Strieder (adelirstrieder@uol.com.br)
6

7 **Abstract**

8 This paper examines the domes and basins, regional arcs and synclines, and brittle structures
9 [in the upper units of São Bento Group \(Paraná Basin\)](#) to characterize the deformational phases
10 in its Jurassic to Cretaceous history. Geometric, kinematic [and dynamic structural](#) analyses
11 [were applied to define](#) two deformational phases. Both developed under regional bi-
12 directional constrictional ($\sigma_1 \geq \sigma_2 \gg \sigma_3$) stress regimes that produced a number of non-
13 cylindrical folds. [The D1 deformational phase](#) produced the N–S and E–W orthogonally
14 oriented domes and basins. The D2 arcs and synclines are oriented towards the NW and NE
15 and indicate a clockwise rotation (35–40°) of both horizontal principal stress tensors.
16 [Stress/strain partition in elongated domes or basins controls lower scale structural elements](#)
17 [distribution](#). The extensional joints and strike-slip faults characterize the local stress field in
18 the outer rim of the orthogonally buckled single volcanic flow, whereas the inner rim
19 supported constriction and developed the local arcuate folds. Fault-slip data inversion was
20 performed using two different techniques to distinguish local and remote stress. [The strike-](#)
21 [slip is a local scale stress regime, resulting from stress drop after the onset of extensional](#)
22 [joints \(orthogonal dykes patterns\) in the outer rim of domes or basins.](#)

Código de campo alterado

Excluído: of the

Excluído: flood volcanism

Excluído: First-stage fieldwork revealed brittle structures, extensional joints, and strike-slip faults, and second-stage fieldwork investigated the connections of the brittle structures to both open folds and dome-and-basin features. Fault-slip data inversion was performed using two different techniques to distinguish local and remote stress/strain.

Excluído: and

Excluído: completed the investigations of the deformation, which characterized

Excluído: for the Jurassic to Cretaceous periods in the Paraná Basin.

Excluído: A

Excluído: of the buckled single flow

Excluído: thus,

Excluído: ¶

Excluído: /strain

1 Introduction

The Paraná Basin is located in the South America Plate (Fig. 1) and is characterized as a huge Paleozoic to Mesozoic intracratonic depression filled by sedimentary and volcanic rocks (see Zalán et al., 1991; and Zalán, 2004 [for a revision on stratigraphy and tectonic subjects](#)). [The upper stratigraphic sequences \(São Bento and Guará groups\) occupy c.a. 80% of the basin area. The São Bento Group is mainly composed by Serra Geral Formation, which contains the volcanic rocks of the well-known Paraná–Etendeka Flood Basalt Province \(Wilson, 1989\).](#) [However, the regional stratigraphic correlation and facies change for the São Bento Group](#) remain controversial, since Scherer and Lavina (2006) correlated the Pirambóia Fm. with Neo-Permian sedimentary units, while Soares et al. (2008a) correlated it with Neo-Triassic to Jurassic sedimentary units. The regional isopach maps for the Mesozoic sedimentary sequence (Artur and Soares, 2002; Soares et al., 2008b) fit well with the results presented here. Thus, the proposition by Soares et al. (2008a) is adopted to characterize the Jurassic–Cretaceous stratigraphic interval of the Paraná Basin. As a result, the São Bento Group is considered to comprise the Pirambóia and Guará (Eo to Meso-Jurassic), Botucatu (Neo-Jurassic), and Serra Geral (Cretaceous) formations (Soares et al., 2008a).

The main structural features of the Paraná Basin were recognized using satellite imagery lineaments and fault plane trends (e.g., Soares et al., 1982; Zeffass et al., 2005; Reginato & Strieder, 2006; Strugale et al., 2007; Machado et al., 2012; Nummer et al., 2014; Jacques et al., 2014), geophysical lineaments (e.g., Ferreira, 1982; Ferreira et al., 1989; Quintas, 1995), or isopach maps developed for each sedimentary sequence (e.g., Northfleet et al., 1969; Artur and Soares, 2002). The main findings include regional lineaments, arcs, and flexures (Fig. 1) that have been summarized by Almeida (1981), Zalán et al. (1991), and Zalán (2004). These authors also highlighted the influence of the basement on the development of these structural features in the Paraná Basin. These regional-scale structural features deform the entire Paraná

Excluído: T

Excluído: uppermost sequences in the Paraná Basin (

Excluído:)

Excluído: The Serra Geral Formation is mainly composed of volcanic rocks, well known as the Paraná–Etendeka Flood Basalt Province (Wilson, 1989).

1 Basin sequence and do not depend on the stratigraphic interpretation of the uppermost
2 sequences.

3 Riccomini (1995) conducted the first paleostress investigation of the uppermost stratigraphic
4 units of the Paraná Basin by applying the method of Angelier and Mechler (1977). Due to the
5 large predominance of the lateral fault-slip data, Riccomini (1995) adopted a strike-slip stress
6 regime to distinguish a number of deformational phases from the Permian units of the Paraná
7 Basin through to the Holocene continental margin rift basins (Table 1). The main criterion to
8 distinguish the deformational phases was, then, to separate fracture direction families with
9 compatible sense of movement. These assumptions and procedures were based on
10 propositions suggesting differential movements during South American and African plate
11 rotation after Gondwana rifting (Morgan, 1983; Chang et al., 1992; Riccomini, 1995).

12 Recent publications also adopted a strike-slip stress regime, following the proposition of
13 Riccomini (1995). Strugale et al. (2007) distinguished two deformational phases in the
14 Jurassic and Cretaceous of the Ponta Grossa Arc region. These deformational phases can be
15 correlated to D_{n+1} and D_{n+2} described by Riccomini (1995). Similarly, Machado et al. (2012)
16 and Nummer et al. (2014) distinguished three deformational phases in the high hills of the
17 Torres Syncline. These phases can also be correlated with the D_n , D_{n+1} , and D_{n+2} phases
18 proposed by Riccomini (1995).

19 Heemann (1997, 2005), Reginato (2003), Acauan (2007), and Amorim (2007) also applied the
20 Angelier and Mechler (1977) method to fault slip data from volcanics and interlayered aeolian
21 sandstones of the Serra Geral Fm. These works adopted geometric and symmetry analysis of
22 fault slip data to distinguish two deformational phases: i) a NS and EW oriented stress field,
23 and ii) a NW and NE oriented stress field. However, some of the observed structural features
24 do not equate for a strike-slip stress regime. Strieder and Heemann (1999) and Reginato and
25 Strieder (2006) highlighted the NS–EW orthogonal pattern of the sandstone dikes and

Excluído: and

Excluído: ed

Excluído: by applying the method of Angelier and Mechler (1977)

Excluído: used

Excluído: Riccomini (1995) interpreted these deformational phases by considering transcurrent regimes, mainly due to the large predominance of striae parallel to the fault strike and

Excluído: ly,

Excluído: However, t

Excluído: ir

Excluído: , which involved a

Excluído: , enabled deformational phases to be distinguished. Consequently, Heemann (1997, 2005), Reginato (2003), Acauan (2007), and Amorim (2007)

Excluído: ed

Excluído: ; howeverbut, they could not determine which of these was the first

mineralized veins emplaced into the basalts. Heemann (1997, 2005), Reginato (2003), Acauan (2007), and Amorim (2007) also identified areas with opposite positioning of the maximum and minimum stress axes (Table 2). Therefore, these results were under evaluation and additional fieldworks for fault slip data, fault geometry analysis and arcuate fold analysis were carried out.

The present paper aims to demonstrate that a bi-directional constrictional stress state regime was active during Jurassic (Botucatu Fm.) and Cretaceous (Serra Geral Fm.) periods in the Paraná Basin. This stress state regime was determined by means of structural analysis techniques from a number of local and regional structural elements used to characterize the deformational phases.

The structural analysis follows Turner & Weiss (1963, p. 3-11). The geometric analysis is developed for outcrop and regional scale folds, domes and basins, and also for fractures (joints and faults). The kinematic analysis is based on paleostress inversion, but its results are reconciled with geometry and symmetry of fractures. The dynamic analysis of the deformation integrates geometric and kinematic analyses for both folds and fractures, in order to define the deformational regime, the structural relationships between folding and fracturing, stress drop and tensor permutation, and the development of orthogonal joint pattern.

2 Fieldwork and structural analysis methods

The fieldworks were carried out in three research stages to record structural features in the volcanic rocks and intertrap sandstones of the Serra Geral Fm., and in the Botucatu Fm. sanstones, mainly at the contact of these formations. The investigated structural features include: fault plane, slip direction and sense, type of kinematic indicator, fault splay

Excluído: , although their findings were difficult to interpret

Excluído: need to be investigated further using

Excluído:

Excluído: and

Excluído: This ¶ study aimed to reports the results of a large-scale structural analysis survey conducted within the Serra Geral and the underlying Botucatu formations. An analysis of the brittle structures focused mainly on stress inversion techniques applied to fault-slip data from volcanic rocks in order to distinguish the different phases of deformation and evaluate the paleostress field during the Jurassic to Cretaceous periods.¶

The paper presents a geometrical and kinematical analysis of mesoscale faults (10–100-m long) investigatstudied at 42 sites (quarries and large road cuts) located within the central region and eastern border of the Paraná Basin.

Excluído: e symmetry, geometric, kinematic and dynamic analysis incorporate o constrain their times of occurrence,

Excluído: were used

Excluído: se

Excluído: : fault plane, slip direction and sense, type of kinematic indicator, fault splay geometry, fracture opening and infilling, large-scale folding and dome-and-basin features, and the basal contact of the Botucatu and Serra Geral formations

Excluído: and, finally,

Excluído: ¶

Excluído: The paper also discusses the stress state regime tectonic conditions within which the paleostress axis inversion operated and the orthogonal joint pattern developed. In this way, the dynamic analysis discusses the operation of local and far (remote) stress field in development of the structural elements. Orthogonal joint formation and its associated stress inversion remain subjects of discussion, and a number of mechanisms have been proposed to account for the local and regional deformational features (see Caputo, 1995; Caputo and Hancock, 1999; Bai et al., 2002). Based on these elements, the mesoscale fault geometries and fault-slip data of the rocks of the Serra Geral Fm. have been shown to be reliable indicators of the distribution of the local paleostress state in the Paraná Basin during the Jurassic to Cretaceous periods.¶

Excluído: The regularities of the preliminary paleostress fields

Excluído: ed

1 [geometry, fracture opening and infilling, fold of different scales and dome-and-basin features,](#)
2 [and the basal contact of the Botucatu and Serra Geral formations.](#)
3 [The significance of fault-slip data on this study makes necessary to show explicitly i\) the field](#)
4 [analysis for splaying Riedel fractures geometry and symmetry and the recorded type of striae,](#)
5 [and ii\) the paleostress technique used for fault-slip data inversion.](#)

Excluído: at different sites inspired a second stage of fieldwork, which involved both revisiting previous sites to obtain a more complete structural study and surveying new sites in the southern Paraná Basin.

Excluído: A third stage of fieldwork was performed to characterize the gentle folds and dome-and-basin structures developed within the Botucatu and Serra Geral formations. The procedure for characterizing such structures involved their identification from satellite imagery or aerial photographs, followed by fieldwork to measure the sandstone–basalt contact orientations, or the basal surface of a given basalt flow.

7 2.1. Fieldwork methods for brittle structures

8 The [brittle structural features were investigated](#) in open-pit quarries, underground openings,
9 and large road cuts ([mesoscale faults: 10–100-m long](#)). This investigation [were carried out in](#)
10 42 sites, [and](#) involved analysis of the slip direction and sense of movement of more than 800
11 fault planes. To ensure the confidence of the results, only those records with a clearly defined
12 slip sense were sampled for the computation of the paleostress fields. [Brittle structures were](#)
13 [recorded in basalts, andesites and dacites of the Serra Geral Fm., since kinematic indicators](#)
14 [are best preserved in these lithologies.](#)

Excluído: structural geological studies were undertaken

Excluído: e

Excluído: of the brittle structures from the

15 Field investigations also included geometrical data records based on fracture splaying (Fig. 2).
16 Fracture splaying shows patterns similar to synthetic [and antithetic](#) fractures developed during
17 shear experiments (e.g., Tchalenko, 1970; Tchalenko and Ambraseys, 1970). Most fracture
18 patterns exhibit open spaces and at least one of those fractures is mineralized. [The fracture](#)
19 [patterns, mineralization of dilatational spaces and sandstone dikes](#) can be observed on
20 different scales, but their geometric relationships are more easily distinguished on the outcrop
21 scale. A field diagram was developed to compile and record different fracture patterns (Fig.
22 3).

Excluído: Mineralization is composed of carbonate, chalcidony, and zeolites, or a combination of carbonate + chalcidony + celadonite.

Excluído: and

23 Kinematic indicators include a variety of types, but frictional steps and the accretionary
24 growth of crystal fibers (Hancock, 1985), and RM and TM types of secondary fracture steps
25 (Petit, 1987) largely predominate (Fig. 4). Some fault planes display different slip striations

and movements, and occasionally crosscutting (truncation) relations could be recorded (Fig. 4B). The truncation between different striations in the same plane suggests their age relation (Table 3). A rare melted and polished fault plane with slip striae is shown in Fig. 4C and ductile drag deformation of the horizontal joints can be observed in Fig. 4D in the basaltic rock with the development of a fracture cleavage.

2.2. Methods for evaluation of deformational phases in the Serra Geral Fm.

The first approximations for paleostress regimes in the volcanic rocks of the Paraná Basin used the graphical method described by Angelier and Mechler (1977). This graphical method superposes P and T dihedrals for each element of fault-slip data, which allows paleostress regimes to be distinguished by grouping compatible fracture splay geometries and fault slip data.

In the second phase of the paleostress analysis, the above graphical method was combined with two numerical stress-inversion techniques (Žalohar and Vrabec, 2007, 2008), by means of the T-TECTO 3.0 program (http://www2.arnes.si/~jzaloh/t-tecto_homepage.htm) developed by Dr. Jure Žalohar. The Gauss method is an inverse-method that is applied to define paleostress (Žalohar and Vrabec, 2007), whereas the MSM is used as the direct kinematic paleostrain method (Žalohar and Vrabec, 2008). The parameters for stress inversion by MSM are shown in Table 4.

The Gauss method was applied site-by-site to limit the fault-slip data numbers and to evaluate local heterogeneities in the paleostress regimes of the Paraná Basin volcanic rocks. It is important to note that the Gauss method can distinguish between heterogeneous fault-slip data, as is the present case (two superposed deformational phases).

In order to obtain numerically stable results, the fault-slip data of some sites were merged based on their proximity, fault-slip consistency, geometry, and fault pattern. The merged

Excluído: a

Excluído: The separation of paleostress regimes from heterogeneous fault systems is tedious. In the present case, the complete fault-slip data sets were tested by applying the Gauss method described by Žalohar and Vrabec (2007). This method defines a Gaussian compatibility function based on the adjustment measure between the angular misfit and the normal to the shear stress ratio on the fault plane.

Excluído: The Gauss method proposed by Žalohar and Vrabec (2007) can distinguish between heterogeneous fault-slip data, as is the present case.

Excluído: Then, the Gauss method was applied site-by-site to limit the fault-slip data numbers and to evaluate local heterogeneities in the paleostress regimes of the Paraná Basin volcanic rocks.

1 fault-slip data represent small areas of the Paraná Basin under homogeneous stress/strain
2 conditions. These fault-slip data were then reprocessed and the results used for the structural
3 analysis discussion.

4 **3 Regional structural features in the Jurassic–Cretaceous units of the Paraná** 5 **Basin**

6 Figure 1 shows some structural features that affect the stratigraphic units of the entire Paraná
7 Basin; however, some are of particular interest with regard to the Jurassic–Cretaceous interval
8 because it will be shown here that they were developed during the deformational phases.

9 The most prominent structures are the large-scale anticlinal and synclinal gentle folds in the
10 eastern border of the Paraná Basin (Fig. 5), which show NW-dipping hinges (see Zalán et al.,
11 1991). Erosion of the anticlines created the area in which the volcanic and sedimentary rocks
12 of the Paraná Basin are exposed towards the NW, and gave rise to the Rio Grande and Ponta
13 Grossa arcs. However, the folds are not cylindrical, but produce elliptical domes and basins
14 (details in Fig. 5).

15 The presence of large domes in the Serra Geral volcanics has long been reported (e.g., Lisboa
16 and Schuck, 1987; Schuck and Lisboa, 1988; Rostirolla et al., 2000). Similar structures were
17 also described for underlying sedimentary sequences (Riccomini, 1995). Close examination of
18 these structural features reveals that they are an association of gentle domes and basins, which

19 can be classified into two groups based on orientation: a) those with N–S or E–W, and b)
20 those with NW or NE for the longest axis direction. Some examples of such domes are
21 indicated in Fig. 5: a) Quaraí Dome, b) Rivera Crystalline Island, and c) Aceguá Crystalline
22 Island. The longest axis of these domes is <100 km. The Quaraí Dome shows a NE
23 orientation of its longest axis, while the Rivera and Aceguá crystalline islands exhibit EW
24

Excluído: The stress inversion was performed using the T-TECTO 3.0 program (http://www2.arnes.si/~izaloh/t-tecto_homepage.htm) developed by Dr. Jure Žalohar. The paleostress/paleostrain regimes were determined using the Gauss method and kinematic multiple-slip method (MSM) (Žalohar and Vrabec, 2008). The MSM calculates weighting factors for moment tensor summation based on the number and orientation of parallel faults of the same size range, direction of slip along them, and the mean rock properties. The parameters for stress inversion by MSM are shown in Table 4.¶ The reduced tensors calculated by these methods can be interpreted either as the stress or strain tensor. The Gauss method is an inverse-method that is applied to define paleostress (Žalohar and Vrabec, 2007), whereas the MSM is used as the direct kinematic paleostrain method (Žalohar and Vrabec, 2008).

Excluído: orientation

Excluído: orientation

1 orientation. Aboy and Masquellin (2013) presented some structural and sedimentary evidence
2 supporting the uplift of the Rivera Crystalline Island from the Permian period onwards.

3 The basal contact of the Serra Geral Fm. volcanic rocks was measured in a number of
4 outcrops to constrain the deformation related to the NW-dipping anticlines–synclines (Fig.
5 5A). Figure 5B shows that the axes of these continental-scale gentle folds are oriented
6 towards 06/308. A balanced SW–NE structural section (Fig. 6) illustrates the relationships
7 between the anticlines–synclines from Uruguay to São Paulo (Brazil). This regional cross
8 section was balanced as concentric folds (Marshak and Mitra, 1988; pp. 269–302).

9 Structural mapping was conducted in the Quaraí Dome area, close to the Brazil–Uruguay
10 border (Fig. 7A). In this area, the erosion of volcanic flows over the Botucatu Fm. sandstones
11 allows a number of domes and basins with different orientations to be recognized. The most
12 important of these is the Quaraí Dome, because it has the greatest amplitude and it exposes
13 the underlying Botucatu Fm. sandstone. Measurements of the sandstone–basalt contact show
14 that the Quaraí Dome is oriented towards 02/043 (Fig. 7B).

15 North and northwest of the Quaraí Dome, two elongated basins (N–S and E–W, respectively)
16 can be recognized (Fig. 7A). The attitudes of the thin volcanic flows are shown for the E–W-
17 dipping (Fig. 7C) and N–S-dipping (Fig. 7D) long axes for both basins.

18 The N–S-oriented folds were also recognized on the outcrop scale (Fig. 7E). This fold is
19 developed upon the Botucatu Fm. sandstone and it was identified in the inner part of the
20 Quaraí Dome along the BR-293 road. The eolian stratification was deformed around an
21 11/176 folding axis (Fig. 7F).

22 The map in Fig. 7A shows that the domes and basins with the same orientation do not
23 interfere with each other. The folds are described as non-cylindrical and arcuate in map view.
24 The fold tightness varies from gentle (interlimb angle: 170° for small domes and basins, 151°

for the Quaraí Dome, and 159° for regional arcs) to open fold (interlimb angle: 120° for the N–S outcrop fold).

4. Paleostress tensors in the Serra Geral Fm. volcanic rocks

The results of the fault-slip data processing are presented in a sequence of figures for each site/area (Figs. 8 and 9). The figures include the Wulff projection (lower hemisphere) of the brittle fault-slip data, misfit angle histogram, unscaled Mohr diagram for resolved stress on the faults, and a diagram relating the values for the object function (M) and shape of the strain ellipsoid (D). The object function depends on the parameters defined in Table 4, and relates the standard deviation (s) of angular misfit between the direction of slip along the faults (striae) and the shear stress produced by a given tensor. Therefore, its value is used to determine the best orientation of stress tensor for those fault-slip data (Žalohar and Vrabec, 2007).

The structural analysis performed on the Serra Geral Fm. volcanic rocks (Paraná Basin) distinguished two different paleostress fields:

- a) Predominantly N–S-oriented maximum horizontal stress with permutations to the E–W;
- b) Predominantly NE–SW-oriented maximum horizontal stress with permutations to the NW–SE.

In both cases, the intermediate principal stress (σ_2) is subvertical, which explains the prevalence of strike-slip faulting. The crosscutting relations between striations (Table 1) indicate that the N–S maximum horizontal stress is older than the NE–SW stress. This interpretation is also consistent with other structural features such as the elliptical domes.

Excluído: These general orientations for the NE–SW (NW–SE) stress tensors agree with those presented by Riccomini (1995), Strugale et al. (2007), Machado et al. (2012), and Nummer et al. (2014). They differ, however, on processing methodology and kinematic analysis. It should be noted that the area studied by Riccomini (1995) and Strugale et al. (2007) is heavily influenced by the NW–SE Ponta Grossa faults and dikes. Despite final results that are difficult to reconcile, it seems that the D1 faults (deformation) defined by Strugale et al. (2007) correspond to the D2 deformational phase discussed here.¶

4.1. Predominantly N–S-oriented maximum horizontal stress with permutations to the E–W

The maximum (σ_1) and minimum (σ_3) compressive paleostresses are subhorizontal (Fig. 8). These main paleostress axes are oriented close to the N–S and E–W directions and in most cases, the stress ratio (Φ) ranges from 0.10–0.30. The mean misfit angle of the fault-slip data for each site/area is $<15^\circ$ (see Fig. 8), while the standard deviation is $<20^\circ$ (see Table 5). These conditions suggest a strike-slip regime and the observed fault-slip data indicate the presence of conjugate patterns of faults (Fig. 8).

This group of tensors shows the permutations of the maximum (σ_1) and minimum (σ_3) compressive paleostress axes between the N–S and E–W directions. In Fig. 8(A, B, E, and G), the maximum compressive (σ_1) paleostress axis is close to the E–W direction, whereas in Fig. 8(C, D, F, H, and I), the maximum compressive (σ_1) tensor is close to the N–S direction. Such results, recorded in the CODECA quarry (Fig. 6G and 6H), were initially intriguing and demanded a careful re-investigation of the fault-slip at this site. The alternated orientation of the maximum paleostress axis was observed at other sites/areas within the Paraná Basin volcanic rocks. Furthermore, the alternation of the stress tensor occurs in some tectonic regimes (Angelier, 1989) and this aspect will be considered later.

4.2. NE–SW maximum horizontal compression

This group of paleostress tensors is also related to the subhorizontal maximum and minimum compressive stresses, while the intermediate stress axis (σ_2) is subvertical (Fig. 9). The maximum horizontal compressive stress is oriented close to NE–SW and the stress ratio (Φ) ranges from 0.10–0.30. These conditions also suggest a strike-slip stress regime and the presence of a conjugate pattern of faults (Fig. 9).

1 The mean misfit angle of the fault-slip data for each site/area is close to 15° (see Fig. 7) and
2 the standard deviation is $<18^{\circ}$ (see Table 6). Table 6 summarizes the results of the stress
3 inversion for this fault-slip data set.

4 The paleostress tensors also indicate the permutations between the maximum (σ_1) and
5 minimum (σ_3) compressive stress axes from the NE–SW to NW–SE directions in some
6 sites/areas (Santa Rita quarry) (see Fig. 9A–F).

7 8 **5. Geometric and kinematic analyses of deformational structures in the** 9 **volcanic rocks**

10 The regional-scale folds (Fig. 5) and the domes and basins (Fig. 7) discussed in the previous
11 sections show systematic relationships with the fracture patterns (Figs. 8 and 9). Thus, the
12 deformational structures developed within the volcanic rocks of the Serra Geral Fm. are
13 analyzed considering the fracture patterns.

14 The geometric and kinematic analyses of fracture patterns use rose diagrams to classify
15 conjugated and splay fractures observed in each site/area, because the strike-slip stress regime
16 developed subvertical to vertical fractures. This procedure makes it possible to distinguish the
17 synthetic and antithetic fractures and to determine the mean ϕ (internal friction angle; see
18 Jaeger, 1969; Angelier, 1989).

19 20 **5.1. Fracture patterns of N–S paleostress tensors**

21 The fracture patterns developed in the N–S maximum horizontal compression clearly indicate
22 conjugate geometry, as can be seen in Fig. 10. However, it is clear that dextral and sinistral
23 conjugate sets show different spatial distributions (orientations) and frequency.

24 The rose diagrams in Fig. 10 show fracture orientations according to the synthetic Riedel
25 fracture criteria (Tchalenko 1970) and reinforce the field observations (Fig. 2). The rose

1 diagrams indicate the predominance of R-type fractures and some diagrams illustrate the
2 presence of fractures at angles lower than 15–20° relative to the main compressive stress axis
3 (σ_1). These fractures are classified as hybrid joints (Hancock, 1985).

4 R-type fractures usually merge with C-type fractures to develop splay or duplex fracture
5 patterns, and hydraulic breccia are often associated with such dilatational spaces. The
6 dilatational space is filled by a zeolite \pm quartz \pm chalcedony \pm calcite \pm celadonite
7 paragenesis.

8 The geometric and kinematic analyses of the N–S-directed paleostress field also consider the
9 occurrence of tabular dykes of thermally metamorphosed sandstone emplaced into the
10 vesicular basalts (Fig. 11A) of the Serra Geral Fm. sequence. A detailed field survey of their
11 orientation was undertaken in the Salto do Jacuí region. Figure 11B shows that these tabular
12 dykes are predominantly subparallel to the maximum compressive stress axis (σ_1) when it is
13 oriented either to the N–S or to the E–W.

14 In the Caxias do Sul region, the thermally metamorphosed sandstone tabular dykes were
15 measured cutting across the massive basalts of the Serra Geral Fm. Figure 11C shows that
16 such dykes are also oriented to the NE–SW; however, they still show the main distribution in
17 the N–S and E–W directions. In the Caxias do Sul region, a large number of mineralized veins
18 were measured. Figure 11D shows that opened fractures are mainly oriented in the N–S, E–
19 W, and NW–SE directions.

20 The orientation of metamorphosed sandstone dykes in the Salto do Jacui and Caxias do Sul
21 regions are slightly different. For the Salto do Jacui region, the preferred orientation is N10E,
22 whereas in the Caxias do Sul region, it is N10W. However, such differences are in accordance
23 with the local stress field orientations, as can be seen in Fig. 8(C, D, E, G, and H).

24 The sandstone dykes and mineralized veins cutting across the basalts are controlled by an
25 orthogonal pattern of fractures. This observation agrees with the permutations of the

1 maximum (σ_1) and minimum (σ_3) compressive paleostress axes between the N–S and E–W
2 directions, as reported above.

3 This orthogonal pattern (N–S and E–W) is also observed in the Cerro do Jarau giant intertrap
4 dune (Remde, 2013). The orthogonal pattern in the Cerro do Jarau area (Fig. 7A), however, is
5 defined by centimeter-scale veins in the basalts (Fig. 12A), and mainly by millimeter-scale
6 deformation bands in the intertrap Botucatu Fm. sandstone (Fig. 12B). The centimeter-scale
7 veins in the basalts display a “ladder” pattern, or an H-shaped abutment (Hancock 1985),
8 where the N–S veins are longest. In contrast, the deformation bands display a “grid” pattern
9 with mutual crosscutting relationships (Rives et al., 1994). The orthogonal deformation bands
10 are crosscut by shear deformation bands (Fig. 12C), suggesting an initial onset of extensional
11 joints, followed by shear. Figure 12(D and E) shows the rose diagrams for the orthogonal
12 patterns in the basalt and sandstone, respectively, in the Cerro do Jarau area.

14 **5.2. Fracture patterns of NE–SW-directed paleostress field**

15 The geometry of the fractures formed in the NE–SW-directed paleostress field shows an
16 asymmetric distribution for the dextral and sinistral conjugated branches (Fig. 13). This
17 asymmetric distribution of fracture orientation frequency allows them to be classified
18 according to the Riedel shear criteria. However, the fault-slip data for the NE–SW paleostress
19 field show that higher frequency Riedel fractures vary between sites, being classified as either
20 R-type, C-type, P-type, or even hybrid fractures.

21 The rose diagrams for the NE–SW paleostress field are in accordance with field observations
22 of fracture splaying. The R- and C-type fractures usually merge into one another to produce
23 both dextral or sinistral splayed fractures and duplex strike-slip patterns. Such fracture
24 patterns are the locus for mineralization. Fracture surfaces and open dilatational spaces are

1 coated by celadonite \pm chalcedony \pm calcite. Hydraulic breccias are also recognized, but with
2 minor frequency.

3 Some rose diagrams in Fig. 13 indicate the presence of extension to the hybrid joints
4 (Hancock, 1985) and additionally, Fig. 13(E and F) suggests the development of the
5 orthogonal fracture pattern in this second deformational phase. In the Cerro do Jarau giant
6 intertrap dune (Fig. 7A), the N–S orthogonal deformation bands are also superposed by “grid”
7 patterns of orthogonal NE–SW deformation bands (Fig. 14A). Careful measurement and
8 evaluation of the orthogonal patterns at a number of outcrops permitted the construction of a
9 rose diagram for this second generation of deformation bands (Fig. 14B). The dispersion of
10 the orthogonal NE–SW deformation bands also suggests the interplay of extensional and
11 hybrid joints.

12

13 6. [Stress/strain regime analysis of the deformational phases](#)

Excluído: A

14 The paleostress analysis distinguished two different deformational phases in the [upper units of](#)
15 [the São Bento Group](#) (Paraná Basin). The relative ages of the deformational events were
16 established from field observations (Table 1), regional-scale folds (Fig. 5), and domes and
17 basins (Fig. 7). The N–S-oriented stress field was assessed as being older than the NE–SW-
18 oriented stress field deformational phase during the Jurassic to Cretaceous periods.

Excluído: Serra Geral Fm. volcanic rocks

19 The regional-scale folds and the dome-and-basin features (Figs. 5 and 7) were shown to
20 pertain to two distinct groups: i) those with N–S and E–W elongations, and ii) those with NE
21 and NW elongations. These directions are closely related to that determined for the
22 orthogonal fracture patterns and faults in the previous sections. Considering Figs. 5, 7–10, 12,
23 and 13, it can be established that a relationship of symmetry exists between the fractures,
24 faults, and folds of the elongated domes and basins. Thus, the association between buckling

processes and brittle deformation will be further analyzed to define their relationships and role in each deformational phase.

6.1. Folds vs fracture patterns relationships

The presence of gentle domes and basins with their longest axes oriented in orthogonal directions (Section 3) suggests a regime of bi-directional compression ($\sigma_1 \sim \sigma_2 > \sigma_3$). Gosh and Ramberg (1968) and Gosh et al. (1995) performed experimental investigations into the development of domes and basins under constrictional deformation. The field data recorded for São Bento Group upper formations do agree with experimental results in that: i) domes and basins are elongated in orthogonal directions (Fig. 7A); ii) domes and basins of the same deformational phase do not interfere with each other, but merge or abut without crossing (Fig. 7A); and iii) the orthogonal fracture patterns and deformation bands are set parallel and perpendicular to the elongated fold hinge (Fig. 15).

Figure 15 summarizes the symmetry relationships between local and regional scale arcuate folds and fractures (joints and faults). It includes field records and results (Figs. 7–14) for the entire investigated area. These symmetry relationships support the development of fractures as consequence of arcuate fold formation in a bi-directional stress state regime.

6.2. Stress/strain analysis for deformational phases

A constrictional deformation regime is usually characterized by a stress difference ratio close to 1 ($D = \Phi \sim 1$). It is common practice to evaluate the stress state from the stress ratio ($D = \Phi$; Angelier, 1989) and Fig. 16A shows a histogram based on the results of the linear inversion method (Gauss method; Žalohar and Vrabec, 2007). It can be seen that the D ratio shows a wide dispersion for the first deformational phase, varying from 0.8 (area C), to 0.0–0.3 in most of the studied sites.

Excluído: Serra Geral Fm.

1 The stress state for each deformational phase can also be evaluated on the diagram proposed
2 by Lisle (1979). This diagram (Fig. 16B) shows that the stress tensors for each site/area are
3 distributed in a linear pattern. This pattern suggests that the main stress difference ($\sigma_1 - \sigma_3$)
4 remains approximately constant, while σ_2 encompasses most of the variation. The N-S-
5 oriented stress field varies from a multidirectional stress field ($\sigma_1 > \sigma_2 \gg \sigma_3$), towards a
6 field where the major stress tensor is greater than the other two ($\sigma_1 \gg \sigma_2 \geq \sigma_3$). The NE-
7 SW-oriented stress field, however, is constrained to the field where the major compressive
8 tensor is greater than the other two.

9 The Morris and Ferril (2009) diagram analyzes the slip tendency of rock mass discontinuities
10 in terms of effective stress; i.e., the diagram can distinguish the influence of fluid pressure
11 (Fig. 16C). The first deformational phase (N-S paleostress) plots in two separate parallel lines
12 of constant slip tendency ($T_s = 1.3$ and 1.5). These two parallel lines suggest the varying
13 influence of the intermediate stress tensor (σ_2) on the deformation. However, the second
14 deformational phase (NE-SW paleostress) data correlate with a linear equation whose angular
15 coefficient is >-1.0 , which shows the influence of variations of both the σ_1 and σ_2 tensors on
16 the deformation.

17 The fault-slip data inversion also allows the strain condition of the deformational phases to be
18 evaluated (e.g., Marrett and Allmendinger, 1990; Cladouhos and Allmendinger, 1993;
19 Žalohar and Vrabec, 2008). Figure 17 shows the logarithmic diagram for strain ratio derived
20 from the Gauss Method (Žalohar and Vrabec, 2007), and from the MSM (Žalohar and
21 Vrabec, 2008). The MSM allows the strain ratio to be determined from the total displacement
22 gradient tensor of all measured fault sets, weighted by the number of faults in each set,
23 number of fault sets (their symmetry), and resolved shear stress (Žalohar and Vrabec, 2008).

24 The MSM strain values were defined by varying slightly the coefficient of residual friction
25 (ϕ) in the T-Tecto program. Such a procedure brought closer adjustment of the stress (Gauss)

1 and strain (MSM) tensors, because the axis of rotation is closer to a main tensor. Tables 5 and
2 6 show that the coefficients of residual friction (ϕ_2) determined from both the Gauss and
3 MSM inversion techniques are largely similar. The greatest difference in friction coefficient
4 ($7-10^\circ$) is related to those sites/areas with a small number of fault-slip data, or asymmetric
5 fault-slip sets.

6 Figure 17A represents the strain derived from the linear inversion technique and shows that
7 deformation was developed under constrictional conditions. This result is consistent with the
8 remote stress field, as discussed above. However, the strain ratio determined from the MSM
9 shows that both deformational phases could be distinguished based on this parameter, but
10 follow a flattening strain path (Fig. 17B). This flattening strain path results from a local stress
11 field, because most of the investigated sites [for fault-slip data inversion](#) represent a single
12 outcrop.

13 [It must be noted, on the other hand,](#) that the flattening strain path (Fig. 17B) is consistent in
14 the volcanic rocks of the Paraná Basin, even for sites combining two or more outcrops (see
15 Žalohar and Vrabec, 2008). The highest ($\epsilon_2 - \epsilon_3$) MSM strain ratio is achieved in those sites
16 where conjugated faults or symmetric fault sets are best developed (see Fig. 13). Additionally,
17 the flattening strain path is best developed for the second deformational phase, which could
18 be a consequence of the higher degree of fractures inherited from the original basalt flows and
19 the first deformational phase.

20 The strain-ratio diagrams indicate a bi-directional constrictional deformation of the Paraná
21 Basin for both phases. However, a deformational model must be developed to account both
22 for the remote and local stress/strain fields and for the observed fracture patterns.

24 [6.3. Deformational model and the orientation of main horizontal stress tensors](#)

Excluído: However, i

1 The deformational structures under investigation were developed upon [both upper formations](#)
 2 [of the São Bento Group](#) (Paraná Basin). The volcanic flows [are dominantly massive](#), show
 3 large lateral extensions and are usually [more than 20 m](#) thick ([Heemann, 1997, 2005;](#)
 4 [Reginato, 2003; Acauan, 2007; Amorim, 2007](#)). Thus, the buckling deformation must have
 5 been produced by a tangential longitudinal mechanism (Ramsay, 1967, p. 391–415) and the
 6 neutral surface must have played an important role in local strain partitioning and the
 7 development of the [local scale](#) structures. Figure 18, based on the discussion by Lisle (1999),
 8 summarizes a geometric model relating [bi-directional](#) constrictional domes and basins,
 9 orthogonal fracture patterns, deformation bands, and conjugated faults.

10 The relations of symmetry of joints and faults to folds have long been investigated (e.g.,
 11 Stearns, 1978; Hancock, 1985; Cosgrove and Ameen, 1999). The geometry of the domes and
 12 basins in the Paraná Basin volcanics (Fig. 7) has to consider bi-directional constriction in
 13 which both the major and intermediate ($\sigma_1 \geq \sigma_2$) remote tensors are horizontal. The buckling
 14 mechanism operating simultaneously in the orthogonal direction gave rise to a local flattening
 15 strain field in the outer part of the single flows, and open orthogonal extensional joints (Fig.
 16 18). The fault-slip data, orthogonal joints, veins, and deformation bands were measured at the
 17 outcrop scale and then developed to the outer buckled rim of each single volcanic flow of the
 18 [Serra Geral Fm.](#)

19 The elongation ratio [and orientation of the greatest axis](#) of the domes and basins ([arcuate](#)
 20 [folds](#)) [control stress/strain partition and orientation at this scale. Then, at domes and basins](#)
 21 [scale, \$\sigma_{1db}\$ orient parallel to the shortest axis, while \$\sigma_{2db}\$ orient parallel to major axis. The local](#)
 22 [flattening field in the outer rim of dome and basin, however, implies a third order stress/strain](#)
 23 [partition \(\$\sigma_{1or} \gg \sigma_{2or} \geq \sigma_{3or}\$ \). Both these conditions explain the main stress/strain tensor](#)
 24 [permutation recorded in Figures 8 and 9 \(Section 4\): a\) NS and EW \(\$D_1\$ \), and ii\) NW and NE](#)
 25 [\(\$D_2\$ \).](#)

Excluído: the basalts to dacites of the Serra Geral Fm.

Excluído: (>20 m)

Excluído: ; the main part of the basaltic flows are dominantly massive (Heemann, 1997, 2005; Reginato, 2003; Acauan, 2007; Amorim, 2007)

Excluído: Paraná Basin

1 The gentle interlimb angles [of folds](#) do not suggest large departures between the orientations
 2 of the remote [\(upper order\)](#) and local tensors. Thus, even though the magnitudes and spatial
 3 [position](#) of the remote and local tensors differ, the extensional joints closely parallel the main
 4 tensors and the axes of the domes and basins (cross bc and ac joints: Hancock, 1985). This
 5 deformational model accounts for the square (Fig. 2F) or rectangular (Fig. 12A) symmetry of
 6 the orthogonal veins, and for the “grid-type” deformation bands (Figs. 12B and 14A).
 7 The regional distribution of veins and dykes (Fig. 11) is in accordance with this deformation
 8 history for the Paraná Basin. The emplacement of the thermally metamorphosed sandstone
 9 dykes could be attributed to the mobilization of the still unconsolidated sands from the
 10 underlying Botucatu Fm., or from the Botucatu sands interlayered (intertrapped) between the
 11 sequences of lava flows, into orthogonal extensional joints opened in the outer rim of the
 12 buckled volcanic flows.
 13 The shear fractures (hybrid joints and faults) display a conjugated arrangement with regard to
 14 the extensional joints (Figs. 10, 11, 13), but they started to develop just after the orthogonal
 15 fractures. The symmetry of the hybrid joints and faults is related to hk0 patterns in acute or
 16 obtuse angles to the elongated fold axis (Hancock, 1985).

Excluído: ir

Excluído: distributions

Excluído: volcanics

17 18 [6.4. Local scale strike-slip stress regime and the stress drop](#)

Excluído: S

19 The strike-slip stress field determined from the fault-slip data (Sections 4 and 5) for both the
 20 first and second deformational phases appears to be inconsistent with the local flattening
 21 strain field in the outer part of the buckled volcanic flows. The fault-slip data showed that
 22 rather than the major compressive tensor being vertical (σ_{1or}), it was the local intermediate
 23 tensor (σ_{2or}) instead. However, the onset extensional joints induce local stress release in the
 24 σ_{1or} direction and a permutation between the local σ_{1or} and σ_{2or} tensors. [This stress drop](#)
 25 [explains why the main stress difference \(\$\sigma_1 - \sigma_3\$ \) remains approximately constant \(Fig. 16\).](#)

Excluído: compressive

1 The stress/strain main tensor positioning after local stress release ($\sigma_{1sd} > \sigma_{2sd} > \sigma_{3sd}$,
2 intermediate tensor now in vertical position) characterize the strike-slip stress state, and
3 controls strike-slip faults (hk0 fault symmetry pattern) in the Jurassic to Cretaceous
4 formations of the Paraná Basin. These deformational conditions explain the connection of
5 extensional joints and hybrid to shear fractures, as shown in Figs. 2 and 11A.

6 The bi-directional constrictional deformation in the Paraná Basin during the Jurassic to
7 Cretaceous periods, then, accounts for the outcrop-scale alternation of σ_3 (σ_{3sd}) position, i.e.,
8 either N–S or E–W in the first deformational phase, or NE or NW in the second deformational
9 phase. It should be noted that σ_1 (σ_{1sd}) and σ_3 (σ_{3sd}) orientations alternate between different
10 investigation sites. Thus, it can be concluded that σ_1 (σ_{1sd}) and σ_3 (σ_{3sd}) orientations, inverted
11 from fault-slip data, are related to the elongation of the dome-and-basin structures developed
12 in each area.

13 These deformational conditions explain the connection between extensional joints and hybrid
14 to shear fractures, as shown in Figs. 2 and 11A. The extensional joints and their splays to
15 hybrid and shear fractures frequently have hydraulic breccia (Fig. 2). Such a feature points to
16 supra-hydrostatic conditions ($P/P_{grav} > 0.5$) during the deformation, which favor the
17 development of extensional joints. Veins and associated hydraulic breccia are also developed
18 on fractures related to the second deformational phase, i.e., the supra-hydrostatic conditions
19 remained active during this deformational phase.

20 This structural model of the constrictional deformation in the Paraná Basin also accounts for
21 other important features observed in the volcanic flows. Small-scale folds, similar to that in
22 Fig. 7E, are recorded on basal horizontally jointed portions of the volcanic flows (Fig. 19).
23 These small-scale folds are frequently truncated by fracture zones at their limbs. These folds,
24 however, are developed in the inner zone of the dome-and-basin structures, which is the locus
25 for the local constrictional stress/strain in the tangential–longitudinal mechanism (Fig. 19C).

Excluido: generates

Excluido: In fact, the different σ_1 and σ_3 orientations distinguished in Figs. 8 and 9 are not related to local σ_1 and σ_2 permutations on the outer rims of the folded volcanic flows.

Excluido: The bi-directional constrictional ($\sigma_1 \geq \sigma_2 \gg \sigma_3$) stress regime gave rise to orthogonally oriented domes and basins, as shown by Gosh and Ramberg (1968) and Gosh et al. (1995), which controlled the local distribution of extensional joints and strike-slip faults.

Thus, it can be concluded that buckling of a single lava flow gave rise to the distinguishing deformational structures on either side of its neutral surface. At the outer rims, orthogonal extensional joints developed and sandstones dykes were emplaced, while at the inner rims, non-cylindrical folds developed.

6.5. Time constrain to deformation

The fault-slip and structural data for this investigation derive from the Botucatu and Serra Geral formations (upper units of São Bento Group) of the Paraná Basin. Lava flow stratigraphy differs in each of the studied sites/areas (Heemann, 1997, 2005; Reginato, 2003; Acauan, 2007; Amorim, 2007), and it is still not possible to correlate the studied quarries to specified time intervals taking into account stratigraphic elements. However the investigated structural elements (folds, joints and faults) can be time constrained based in some regional features. This time intervals will certainly be refined in future detailed investigation. The onset of the first deformational episode, however, is not constrained by the volcanic flows and underlying Botucatu Fm. The analysis of the thickness distribution for the underlying Meso-triassic sequence (Artur and Soares, 2002), and also for the Pirambóia–Guará and Botucatu formations (lower units of São Bento Group, Soares et al., 2008b) shows a series of N–S elongated and circular structures. These results suggests that the stress field for the first deformational episode might have operated from at least the Triassic (lower bound) to the Early Jurassic period (upper bound) onwards. For structural purposes, geochronological data produced in association with palaeomagnetic studies for volcanic rocks related to the Paraná Basin can improve structural analysis, because it introduces better differentiation between the relative timings of volcanic structures (flows, dykes, and sills).

Excluído: The deformational structures of the volcanic rocks of the Serra Geral Fm. were developed during the Jurassic to Cretaceous periods

Excluído: the fault-slip investigations were constrained to the Serra Geral Fm. volcanics and intertrap sediments, which left the exact time of onset of the first deformational phase to be defined

1 [Palaeomagnetic data and precise absolute ages for Mesozoic basic rocks related to the Serra](#)
 2 [Geral Fm. volcanism clearly distinguish three groups \(see Ernesto, 2006,2009, for a revision\):](#)
 3 [a\) Serra Geral flows, b\) Ponta Grossa Arc and Serra do Mar basic dyke swarms, and c\)](#)
 4 [Florianópolis Dyke Swarm. While some overlap of apparent ages and virtual geomagnetic](#)
 5 [poles \(VGPs\) exists, it should be noted that the Serra Geral flows are older \(time span 135–](#)
 6 [132 Ma\) and show VGPs oriented to 83/090. The Ponta Grossa Dyke Swarm \(PGDS\) shows](#)
 7 [ages spanning from 132–129 Ma and has a mean VGP directed towards 82/059. The](#)
 8 [Florianópolis dykes have a time span in the interval 127–121 Ma and a VGP oriented to](#)
 9 [88/003.](#)

10 [Ponta Grossa Arc and its Dyke Swarm \(PGDS\) are one of the main structural feature of the](#)
 11 [Paraná Basin \(Fig. 5\). The mean axial planes \(305/84\) and arc axes \(06/307\) of these](#)
 12 [structures are all compatible with a mean compressive stress field directed to 035–040 \(D2](#)
 13 [deformational phase\). The mean direction for the basic dykes of the Ponta Grossa Arc is 300–](#)
 14 [310 \(e.g., Strugale et al., 2007\). These structural relationships indicate that the PGDS was](#)
 15 [emplaced in extensional fractures developed at the outer hinge zone in an anticlinal fold \(Fig.](#)
 16 [6\) including Paraná Basin basement. The PGDS crosscut the basement rocks, and sedimentary](#)
 17 [and volcanic rocks of the Paraná Basin \(e.g., Strugale et al., 2007\). In this scenario, the PGDS](#)
 18 [cannot be regarded as an aborted rift arm, as it has previously been interpreted \(e.g., Morgan,](#)
 19 [1971; Chang et al., 1992; Turner et al., 1994\).](#)

20 [The emplacement of the Ponta Grossa dykes \(PGDS\), then, can be taken as the upper age](#)
 21 [limit for the onset of the second deformational episode \(ca. 132 Ma\). And, thus, the first \(D1\)](#)
 22 [deformational phase can be constrained, in a first approximation, to ca. 200–132 Ma interval.](#)
 23 [An upper age limit to D2 deformation can be taken from the emplacement of the](#)
 24 [Florianópolis dykes. Raposo et al. \(1998\) related them to extension of the South America](#)

1 [crust just prior to the Atlantic oceanic crust expansion. Thus, the second \(D2\) deformational](#)
2 [phase can be preliminary constrained to ca. 132–121 Ma interval.](#)

7. Conclusions

5 The geometric, kinematic [and dynamic](#) analyses of field data permitted [to characterize a](#)
6 [regional bi-directional constrictional \(\$\sigma_1 \geq \sigma_2 \gg \sigma_3\$ \) stress state regime](#) during the Jurassic to

7 Cretaceous periods [of the Paraná Basin. Two](#) deformational phases [were](#) developed under
8 [these](#) regional constrictional stress regimes and gave rise to a number of non-cylindrical folds.

9 These structures are characterized as domes and basins, and regional anticlines and synclines.

10 Consequently, both deformational phases produced similar local-scale structures, [that](#) can be
11 distinguished both by the orientation and by some [particular](#) structural features. The first

12 deformational phase shows elongated domes and basins oriented both N–S and E–W. The
13 second deformational phase also shows elongated domes and basins, but these are oriented
14 NW–SE and NE–SW, according to the most expressive Ponta Grossa and Rio Grande arcs,
15 and the Torres Syncline in the eastern border region of the Paraná Basin. These conditions
16 indicate a clockwise rotation (35–40°) for both horizontal principal stress tensors ($\sigma_1 \geq \sigma_2$)
17 during the Cretaceous period.

18 The [stress/strain partition at different scales was responsible for structural features recorded at](#)
19 [decreasing scales in the Paraná Basin. The orthogonal orientation of the major axis of domes](#)
20 [and basins controls alternated orientation of stress/strain tensors \(\$\sigma_{1db} \geq \sigma_{2db}\$ \) at this scale.](#)

21 [The tangential longitudinal buckling mechanism supported by massive, thick volcanic layers](#)
22 [enabled local scale stress/strain partition between outer and inner arcuate folds. The outer rim](#)
23 [developed](#) orthogonal patterns of the dykes and veins, [and also deformation bands,](#) retaining
24 symmetric relationships with the fold axes of the elongated domes and basins. The inner rims
25 of the buckled volcanic flows, however, developed local arcuate folds, whose local stress axes

Excluído: and

Excluído: the

Excluído: two deformational phases

Excluído: to be distinguished

Excluído: ¶

Both

Excluído: bi-directional

Excluído: ($\sigma_1 \geq \sigma_2 \gg \sigma_3$)

Excluído: . However, these deformational phases

Excluído: of their structures

Excluído: other

1 are close to the regional ones. It should be noted that local-scale folds could reproduce the
2 regional bi-directional constrictional regime.

3 The stress/strain condition in the outer rim of arcuate folds (flattening) governs σ_{3sd} position,
4 either N–S or E–W (D1 phase), or NE or NW (D2 phase), after stress drop due to extensional
5 fractures onset. These conditions are supported by the fact that strike-slip faults follow the
6 development of extensional joints. The strike-slip faults are, then, the result of the stress drop
7 after the onset of the extensional joints, which enabled a local scale permutation between σ_{1or}
8 and σ_{2or} .

9 The paleostress orientation derived from fault-slip data, thus, is related to the local stress field
10 developed upon the buckled single volcanic flows of the Serra Geral Fm. after stress drop
11 episodes. The strike-slip stress state regime proposed by Riccomini (1995), Strugale et al.
12 (2007), Machado et al. (2012), and Nummer et al. (2014), then, is a local scale stress field.
13 This strike-slip stress state regime, however, was applied on specific way for data processing
14 methodology and kinematic analysis by those authors. Then, the deformational phases
15 discriminated by Riccomini (1995), Strugale et al. (2007), Machado et al. (2012), and
16 Nummer et al. (2014) are hard to reconcile with results obtained in this study without
17 introducing biased interpretation.

19 Author contribution

20 A.J.S, R.H., P.A.R.R., R.B.A., V.A.A., and M.Z.R participated in the study design and
21 concept, data collection, and data analysis and interpretation during the first stages of the
22 investigation. A.J.S. also supervised all the investigation and conducted the second stage of
23 field work, data analysis and interpretation. A.J.S. wrote the main manuscript, and R.H.,
24 P.A.R.R., R.B.A., V.A.A., and M.Z.R conducted critical review and suggested amendments to
25 the final manuscript.

Excluído: Further investigations are needed to address this point in the future.

Excluído: These orthogonal extensional joints are developed in the outer rims of the folded volcanic flows; however, the strike-slip faults follow the development of extensional joints. The strike-slip faults are the result of the stress drop after the onset of the extensional joints, which enabled a local permutation between σ_1 and σ_2 . The $hk0$ symmetry for the strike-slip faults in the arcuate folds is in accordance with field observations.¶

Excluído: outcrop-scale alternation of the

Excluído: is not related to

Excluído: The different σ_1 and σ_3 orientations distinguished in Figs. 8 and 9 are mainly reported in different investigation sites and result from the orientation of the arcuate fold minor axis. Thus, the σ_3 position depends on the orientation of the orthogonal elongated domes and basins. Thus, further investigation is in progress to determine the regional (remote), rather than local stress/strain field in the Jurassic to Cretaceous periods of the Paraná Basin.¶ These orthogonal extensional joints are developed in the outer rims of the folded volcanic flows; however, the

Excluído: The $hk0$ symmetry for the strike-slip faults in the arcuate folds is in accordance with field observations.

Excluído: The paleostress-inversion-based distinction of fracture orientation families introduces biased results in some previous papers. The field-based data (fault-slips, fracture patterns, dykes, and contact attitudes) and data derived from paleostress inversions and kinematic analyses are in agreement with each of the deformational phases.¶

Excluído: however

Excluído: ¶

Excluído: se general orientations for the NE–SW (NW–SE) stress tensors agree with those presented

Excluído: e

Excluído: y differ

Excluído: It should be noted that the area studied

Excluído: and

Excluído: is heavily influenced by the NW–SE Ponta Grossa faults and dikes. Despite final results that are difficult

Excluído: , it seems that the D1 faults (deformation) defined by Strugale et al. (2007) correspond to the D2 deformational phase discussed here

Excluído: The Gauss and MSM paleostress inversion methods (Zalohar and Vrabec, 2007, 2008) were applied to fault-slip data for 42 sites in the southeast border and central regions of the Paraná Basin (Brazil). A number of fieldwork campaigns were undertaken to map the important structural features of the Paraná Basin that developed during the Jurassic to Cretaceous periods.¶

1
2
3
4
5
6
7
8
9
10
11
12
13
14

Acknowledgments

The authors especially thank Dr. Jure Žalohar for kindly providing a license for the T-Tecto 3.0 software (http://www2.arnes.si/~jzaloh/t-tecto_homepage.htm), and for reading the article and offering comments and suggestions for its improvement. The authors also thank Dr. Luis Eduardo S.M. Novaes and Dr. Bardo Bodmann for their comments regarding this work. We also extend our gratitude to the Referee 1 for their careful consideration and comments that have helped us improve the quality of the article. The authors thank the Brazilian research agencies (FAPERGS, CNPq, CAPES, FINEP) for supporting the initial projects regarding the Paraná Basin volcanic rocks, and the Universidade Federal de Pelotas for supporting and encouraging the more recent local and regional fieldwork campaigns.

References

- Aboy, M., and Masquellin, H.: Relações embasamento vs. cobertura na Ilha Cristalina de Rivera, Uruguai, in: Simpósio Sul-brasileiro de Geologia, Abstracts, SBG, Porto Alegre (Brazil), 126, 2013.
- Acauan, R. B.: Geologia e controle estrutural das ocorrências de ágatas e ametistas na região de Quaraí/Santana do Livramento (RS). Master degree Dissertation, PrPG em Engenharia de Minas, Metalurgia e Materiais, UFRGS, Brazil, 167 pp., 2007.
- Almeida, F. F. M.: Síntese sobre a tectônica da Bacia do Paraná, in: Simp. Regional de Geologia, 3, SBG-SP, Curitiba (Brazil), 1, 1–20, 1981.
- Amorim, V. A.: Modelagem geológica e controle dos depósitos em geodos no Distrito Mineiro de Ametista do Sul (RS, Brasil). Master degree Dissertation, PrPG em Engenharia de Minas, Metalurgia e Materiais, UFRGS, Brazil, 173 pp., 2007.
- Angelier, J.: From orientation to magnitudes in paleostress determinations using fault slip data. *J. Struct. Geol.*, 11, 37–50, 1989.
- Angelier, A. and Mechler, P.: Sur une méthode graphique de recherche de contraintes principales également utilisable et en séismologie: la méthode des diédres droits. *Bull. Soc. Geol. Fr.*, 19, 1309–1318, 1977.
- Artur, P. C. and Soares, P. C.: Paleoestruturas e petróleo na bacia do Paraná, Brasil. *Revista Brasileira de Geociências*, 32, 433–448, 2002.
- Bai, T., Maerten, L., Gross, M. R. and Aydin, A.: Orthogonal cross joints: do they imply a regional stress rotation? *J. Struct. Geol.*, 24, 77–88, 2002.
- Caputo, R.: Evolution of orthogonal sets of coeval extension joints. *Terra Nova*, 7, 479–490, 1995.
- Caputo, R. and Hancock, P. L.: Crack-jump mechanism and its implications for stress cyclicity during extension fracturing. *J. Geodyn.*, 16, 34–59, 1999.

1 Chang, H. K., Kowsmann, R. O., Figueiredo, A. M. F. and Bender, A. A.: Tectonics and
2 stratigraphy of the East Brazil rift system: an overview. *Tectonophysics*, 213, 97–138,
3 1992.

4 Cladouhos, T. T. and Allmendinger, R. W.: Finite strain and rotation from fault-slip data. *J.*
5 *Struct. Geol.*, 15, 771–784, 1993.

6 Cosgrove, J. W. and Ameen, M. S.: A comparison of the geometry, spatial organization and
7 fracture patterns associated with forced folds and buckled folds. *Geol. Soc. Spec.*
8 *Publ.*, 169, 7–22, 1999.

9 [Ernesto, M.: Drift of South American Plate since Early Cretaceous: reviewing the Apparent](#)
10 [Polar Wander path. *Geociências*, 25, 83–90, 2006.](#)

11 [Ernesto, M.: Contribuições dos estudos paleomagnéticos ao entendimento da abertura do](#)
12 [Atlântico. *Boletim de Geociências da PETROBRAS*, 17, 353–363, 2009.](#)

13 Ferreira, F. J. F.: Integração de Dados Geofísicos e Geológicos: Configuração e Evolução
14 Tectônica do Arco de Ponta Grossa. Dissertação de Mestrado, PPG em Geoquímica e
15 Geotectônica, IG-USP, São Paulo (Brasil), 273 pp., 1982.

16 Ferreira, F. J. F.; Monma, R.; Campanha, G. A. C. and Galli, V. L.: Na estimate of the degree
17 of crustal extension and thinning associated with the Guapiara Lineament based on
18 aeromagnetic modelling. *Boletim IG-USP, Série Científica*, 20, 69–70, 1989.

19 Gosh, S. K. and Ramberg, H.: Buckling experiments on intersecting fold patterns.
20 *Tectonophysics*, 5, 89–105, 1968.

21 Gosh, S. K., Khan, D. and Sengupta, S.: Interfering folds in constrictional deformation. *J.*
22 *Struct. Geol.*, 17, 1361–1373, 1995.

23 Hancock, P. L.: Brittle microtectonics: principles and practice. *J. Struct. Geol.*, 7, 437–457,
24 1985.

Formatado: Inglês (Reino Unido)

Formatado: Português (Brasil)

Formatado: Português (Brasil)

- 1 Heemann, R.: Geologia, controles e guias prospectivos dos depósitos de ágata na região de
2 Salto do Jacuí (RS). Master degree Dissertation, PrPG em Engenharia de Minas,
3 Metalurgia e Materiais, UFRGS, Brazil, 107 pp., 1997.
- 4 Heemann, R.: Modelagem exploratória estrutural e tridimensional para a prospecção dos
5 depósitos de ágata do Distrito Mineiro de Salto do Jacuí (RS). PhD thesis, PrPG em
6 Engenharia de Minas, Metalurgia e Materiais, UFRGS, Brazil, 163 pp., 2005.
- 7 Jacques, P. D.; Machado, R.; Oliveira, R. G.; Ferreira, F. J. F.; Castro, L. G. and Nummer, A.
8 R.: Correlation of lineaments (magnetic and topographic) and Phanerozoic brittle
9 structures with Precambrian shear zones from the basement of the Paraná Basin, Santa
10 Catarina State, Brazil. *Bra J Geol*, 44, 39–54, 2014.
- 11 Jaeger, J. C.: Elasticity, Fracture and Flow: with Engineering and Geological Applications.
12 Chapman & Hall, London, 268 pp., 1969.
- 13 Leinz, V., Bartorelli, A. and Isotta, C. A. L.: Contribuição ao estudo do magmatismo basáltico
14 Mesozóico da Bacia do Paraná. *Academia Brasileira de Ciências*, 40, 167–181, 1968.
- 15 Lisboa, N. A. and Schuck, M. T. G. O.: Identificação de padrões estruturais no Grupo São
16 Bento, Quaraí, RS, através de imagens orbitais e sub-orbitais. *Pesquisas em*
17 *Geociências*, 20, 5–23, 1987.
- 18 Lisle, R. J.: The representation and calculation of the deviatoric component of the geological
19 stress tensor. *J. Struct. Geol.*, 1, 317–321, 1979.
- 20 Lisle, R. J.: Predicting patterns of strain from three-dimensional fold geometries: neutral
21 surface folds and forced folds. *Geol. Soc. Spec. Publ.*, 169, 213–221, 1999.
- 22 Machado, R.; Roldan, L. F.; Jacques, P. D.; Fassbinder, E. and Nummer, A. R.: Tectônica
23 transcorrente Mesozoica-cenozóica no Domo de Lages – Santa Catarina. *Revista*
24 *Brasileira de Geociências*, 42, 799–811, 2012.

Excluído: i

- 1 Marrett, R. and Allmendinger, R. W.: Kinematic analysis of fault-slip data. *J. Struct. Geol.*, 12
2 973–986, 1990.
- 3 Marshak, S. and Mitra, G.: Basic methods of structural geology. Prentice Hall, New Jersey
4 (USA), 446 pp., 1988.
- 5 Meirelles, M. C.: Determinação da resistência ao cisalhamento de enrocamentos da UHE
6 Machadinho através de ensaios de cisalhamento direto de grandes dimensões. Master
7 degree Dissertation, PrPG Engenharia Civil, UFSC, Brazil, 123 pp., 2008.
- 8 [Morgan, W. J.: Convection plumes in the lower mantle. *Nature*, 230, 42–43, 1971.](#)
- 9 Morgan, W. J.: Hotspot tracks and the early rifting of the Atlantic. *Tectonophysics*, 94, 123–
10 139, 1983.
- 11 Morris, A. P. and Ferrill, D. A.: The importance of the effective intermediate principal stress
12 (σ_2) to fault slip patterns. *J. Struct. Geol.*, 31, 950–959, 2009.
- 13 Northfleet, A. A., Medeiros, R. A. and Mühlmann, H.: Reavaliação dos dados geológicos da
14 Bacia do Paraná. *Boletim Técnico da PETROBRAS*, Rio de Janeiro, 12, 291–346,
15 1969.
- 16 Nummer, A. R., Machado, R. and Jacques, P. D.: Tectônica transcorrente
17 mesozoica/cenozoica na porção leste do Planalto do Rio Grande do Sul, Brasil.
18 *Pesquisas em Geociências*, 41, 121–130, 2014.
- 19 Petit, J. P.: Criteria for the sense of movement on fault surfaces in brittle rocks. *J. Struct.*
20 *Geol.*, 9, 597–608, 1987.
- 21 Quintas, M. C. L.: O embasamento da Bacia do Paraná: reconstrução geofísica de seu
22 arcabouço. Tese de Doutorado, PPG em Geofísica (IAG-USP), São Paulo (SP),
23 213 pp., 1995.
- 24 Ramsay, J.: Folding and fracturing of rocks. McGraw-Hill, New York, 568 pp., 1967.

- 1 [Raposo, M. I. B., Ernesto, M., and Renne, P. R.: Paleomagnetism and \$^{40}\text{Ar}/^{39}\text{Ar}\$ dating of the](#)
2 [Early Cretaceous Florianópolis dike swarm \(Santa Catarina Island\), Southern Brazil.](#)
3 [Earth and Planetary Science Letters, 108, 275–290, 1998.](#)
- 4 Reginato, P. A. R.: Integração de dados geológicos para prospecção de aquíferos fraturados
5 em trecho da Bacia Hidrográfica Taquari-Antas (RS). PhD thesis, PrPG em
6 Engenharia de Minas, Metalurgia e Materiais, UFRGS, Brazil, 286 pp., 2003
- 7 Reginato, P. A. R and Strieder, A. J.: Caracterização estrutural dos aquíferos fraturados da
8 Formação Serra Geral na região nordeste do Estado do Rio Grande do Sul. Revista
9 Brasileira de Geociências, 36, 13–22, 2006.
- 10 Remde, M. Z.: A megaduna intertrap do Cerro do Jarau (RS). Bachelor degree Dissertation,
11 Engenharia Geológica, CDTec-UFPel, 95 pp., 2013.
- 12 Riccomini, C.: Tectonismo gerador e deformador dos depósitos sedimentares pós-
13 gondvânicos da porção centro-oriental do Estado de São Paulo e áreas vizinhas. Tese
14 de Livre Docência, Instituto de Geociências, Universidade de São Paulo, São Paulo
15 (Brasil), 100 pp., 1995.
- 16 Rives, T., Rawnsley, K. D. and Petit, J. P.: Analogue simulation of natural orthogonal joint set
17 formation in brittle varnish. J. Struct. Geol., 16, 419–429, 1994.
- 18 Rostirolla, S. P., Assine, M. L., Fernandes, L. A. and Artur, P. C.: Reativação de
19 Paleolineamentos durante a evolução da Bacia do Paraná - O Exemplo do Domo de
20 Quatiguá. Revista Brasileira de Geociências, 30, 639–648, 2000.
- 21 Scherer, C. M. S. and Lavina, E. L. C.: Stratigraphic evolution of fluvial-eolian succession: the
22 example of the Upper Jurassic-Lower Cretaceous Guarú and Botucatu formations,
23 Paraná Basin, Southern Brazil. Gondwana Res., 9, 475–484, 2006.
- 24 Schobbenhaus, C. and Bellizzia, A.: Geological Map of South America. 1:5.000.000 CGMW
25 – CPRM – DNPM – UNESCO, Brasília (Brazil), 2001.

Formatado: Inglês (Reino Unido)

Formatado: Inglês (Reino Unido)

Formatado: Inglês (Reino Unido)

Formatado: Inglês (Reino Unido)

Formatado: Português (Brasil)

Formatado: Português (Brasil)

- 1 Schuck, M. T. G. O. and Lisboa, N. A.: Caracterização de formas e padrões estruturais no
2 Grupo São Bento da Bacia do Paraná no Rio Grande do Sul em imagens orbitais e sub-
3 orbitais. *In: Simpósio Brasileiro de Sensoriamento Remoto*, 1988, Natal (Brazil),
4 *Anais*, 2, 323–333, 1988.
- 5 Soares, A. P., Barcellos P. E., Csordas S. M., Mattos, J. T., Balieiro, M. G. and Meneses, P.
6 R. Lineamentos em imagens de Landsat e Radar e suas implicações no conhecimento
7 tectônico da Bacia do Paraná, in: *Simp. Bras. Sens. Remoto*, 2, Brasília, 143–168,
8 1982.
- 9 Soares, A. P., Soares, P. C. and Holz, M.: Correlações conflitantes no limite Permo-Triássico
10 no sul da Bacia do Paraná: o contato entre duas superseqüências e implicações na
11 configuração espacial do Aquífero Guarani. *Pesquisas em Geociências*, 35, 115–133,
12 2008a.
- 13 Soares, A. P., Soares, P. C. and Holz, M.: Heterogeneidades hidroestratigráficas no Sistema
14 Aquífero Guarani. *Revista Brasileira de Geociências*, 38, 598–617, 2008b.
- 15 Stearns, D. W.: Faulting and forced folding in the Rocky Mountain foreland. *Geol. Soc. Am.*
16 *Mem.*, 151, 1–38, 1978.
- 17 Strieder, A. J. and Heemann, R.: Análise geométrica de estruturas de sucessão vulcânica
18 associada aos depósitos de Ágata do Distrito Mineiro do Salto do Jacuí (RS), in:
19 *Simpósio Nacional de Estudos Tectônicos, Extended Abstracts*, 1, Lençóis (BA), 14–
20 16, 1999.
- 21 Strugale, M., Rostirolla, S. P., Mancini, F., Portela Filho, C. V., Ferreira, F. J. F. and Freitas,
22 R. C.: Structural framework and Mesozoic–Cenozoic evolution of Ponta Grossa Arch,
23 Paraná Basin, southern Brazil. *J. S. Am. Earth Sci.*, 24, 203–227, 2007.
- 24 Tchalenko, J. S.: Similarities between shear zones of different magnitudes. *Geol. Soc. Am.*
25 *Bull.*, 81, 1625–1640, 1970.

- 1 Tchalenko, J. S. and Ambraseys, N. N.: Structural analysis of the Dasht-e Bayaz (Iran)
2 earthquake fractures. Bull. Geol. Soc. Am., 81, 41–60, 1970.
- 3 [Turner, F. J. and Weiss, L. E.: Structural analyses of metamorphic tectonites. McGraw-Hill](#)
4 [Book Company Inc., New York \(USA\), 536 pp., 1963](#)
- 5 [Turner, S., Regelous, M., Kelley, S., Hawkesworth, C., and Mantovani, M.: Magmatism and](#)
6 [continental break-up in the South Atlantic: high precision \$^{40}\text{Ar}\$ - \$^{39}\text{Ar}\$ geochronology.](#)
7 [Earth Planetary Science Letters, 121, 333–348, 1994.](#)
- 8 Wilson, M.: Igneous petrogenesis: a global tectonic approach. Chapman & Hall Ed., London
9 (UK), 466 pp., 1989
- 10 Zalán, P. V.: Evolução Fanerozóica das bacias sedimentares brasileiras, in: Neto, V.M.,
11 Bartorelli, A., Carneiro, C.d.R. and Brito-Neves, B.B., A Geologia do Continente Sul-
12 americano, Editora Beca, São Paulo (Brazil), 595–613, 2004.
- 13 Zalán, P. V., Wolff, S., Astolfi, M. A. M., Vieira, I. S., Conceição, J. C. J., Appi, V. T., Neto,
14 E. V. S., Cerqueira, J. R. and Marques, A.: The Paraná Basin, Brazil. AAPG Memoir.,
15 51, 681–707, 1991.
- 16 Žalohar, J. and Vrabec, M.: Paleostress analysis of heterogeneous fault-slip data: the Gauss
17 method. J. Struct. Geol., 29, 1798–1810, 2007.
- 18 Žalohar, J. and Vrabec, M.: Combined kinematic and paleostress analysis of fault-slip data:
19 the multiple-slip method. J. Struct. Geol., 30, 1603–1613, 2008.
- 20 Zerfass, H., Chemale Jr, F. and Lavina, E. L. C.: Tectonic control of the Triassic Santa Maria
21 Supersequence of the Paraná Basin, Southernmost Brazil, and its correlation to the
22 Waterberg Basin, Namibia. Gondwana Res., 8, 163–176, 2005.

Formatado: Inglês (Reino Unido)

1 Table 1 Deformational phases distinguished in the uppermost units of the Paraná and in the
2 continental rift basins of Southeast Brazil (Riccomini 1995)

Def Phase	Time interval	Main geological features	Interpretation
D _n	Permian to Lower Cretaceous	Deformational event previous to Gondwana rupture NE-oriented basalt and clastic dikes Geophysical alignments	NW-oriented minimum stress (σ_3) axis
D _{n+1}	Upper Cretaceous	NW-oriented basalt dikes in the Ponta Grossa Arc region Final stages of the Serra Geral volcanism Jacupiranga Alkaline Intrusion Anticlinal dome structures	<i>NE basalt dikes and NW Ponta Grossa dikes were indicated to represent a triple junction remnant</i> NE-oriented minimum stress (σ_3) axis Dextral transcurrent system
D _{n+2}	Paleocene to Eocene	Bauru Basin structural development Rift (graben) basins at the continental margin NE-oriented lamprophyric dikes	NW-oriented minimum stress (σ_3) axis Sinistral transcurrent system
D _{n+3}	Eocene to Oligocene	Jaboticabal Alkaline Intrusion Hydrothermal silicification contemporaneous to sedimentation of Itaquari Fm.	NNW-oriented maximum stress (σ_1) axis Dextral transcurrent system
D _{n+4}	Miocene	Ultrabasic flows in Volta Redonda and Itaboraí Deposition of Itaquaquecetuba Fm.	Maximum stress (σ_1) axis alternating from NS and EW according the balance between South Atlantic drifting and Nazca Plate subduction
D _{n+5}	Pliocene	Sinistral EW transcurrent system	
D _{n+6}	Pleistocene to Holocene	NS-oriented grabens Extensional WNW-ESE regime	

1 Table 2 Paleostress fields defined by Heemann (1997, 2005), Reginato (2003), Acauan (2007)
2 and Amorim (2007) for fault slip data of Serra Geral Fm using the method of Angelier and
3 Mechler (1977). [Structural elements notation in this paper follows the Right Hand Rule](#)
4 [\(RHR\)](#).

	(σ_1)	(σ_2)	(σ_3)
Heemann (1997,2005), Heemann and Strieder (1999)			
Salto do Jacuí and Sobradinho region (RS)			
Estrela Velha – Arroio do Tigre área	20-341	35-100	08-219
Sobradinho to Ibarama área	11-321	67-182	02-095
Saltinho área	06-334	72-218	02-120
	12-151	50-044	34-260
Eng. Maia Filho Damp area	04-343	30-250	58-095
	46-357	22-110	13-209
Angico Quarry	36-349	05-255	52-157
Poço Grande Quarry	19-358	14-091	12-178
Zubi and Ralph Quarries	67-341	04-079	23-172
	62-313	15-073	06-165
Pedreira Funda Quarry	50-332	07-086	05-171
Reginato (2003), Reginato and Strieder (2006)			
Caxias do Sul and Veranópolis region (RS)			
Pedreira Guerra Quarry	10-074	80-256	03-346
CODECA Quarry	01-174	86-084	04-264
	03-263	88-092	02-357
Tega Outcrop and Road cut	15-073	72-270	04-165
Veranópolis roadcut	10-068	80-248	02-158
Acauan (2007)			
Santana do Livramento and Quaraí region (RS)			
Santa Rita Quarry	11-032	87-182	07-301
	08-133	80-272	07-042
Registro Quarry	09-116	80-270	04-026
Amorim (2007)			
Ametista do Sul and Frederico Westphalen region (RS)			
Ametista do Sul quarries	25-028	54-330	23- 115
Frederico Westph to Caiçara area	13-110	68-327	17-204
	09-170	72-328	17-083
	20-205	60-334	21-114
Rodeio Bonito Quarry	09-147	70-355	18-241
	29-232	54-355	21-139

Table 3 Summary of crosscutting relations of different striations observed in the same fault

plane

Site	Relative age	Fault plane	Striae orientation	Sense of movement
Pedreira Quarai	1 st	359/73	20/173	Sinistral
	2 nd	359/73	14/006	Dextral
Pedreira SF Assis	1 st	066/72	27/236	Dextral
	2 nd	066/72	27/077	Sinistral
Pedreira Painel	1 st	166/72	09/343	Dextral
	2 nd	166/72	10/169	Dextral
	1 st	034/74	13/039	Sinistral
	2 nd	034/74	60/185	Normal

1 Table 4 Parameters for stress inversion using multiple-slip method (Žalohar and Vrabec
 2 2008).

Parameter	Value range
Dispersion (<i>s</i>)	20
Threshold (Δ)	40–50
Shear strength (ϕ 1)	50–65
Angle of residual friction (ϕ 2)	20–35
Stress parameter	40–50
Andersonian regime set	Yes

3 The shear strength and angle of internal friction data for volcanic rocks of Paraná Basin are
 4 from fresh rock test (Meirelles 2008).

5

6 Table 5 Summary of principal stress axes in the N–S and E–W orientations computed for sites within the volcanic rocks of the Paraná Basin.

Site	Standard deviation of s	Linear inversion							MSM inversion						
		σ_1	σ_2	σ_3	Relative values of λ_i	D	ϕ_2	σ_1	σ_2	σ_3	Relative values of λ_i	D	ϕ_2		
A Compilation from PR (Ped Registro) and PQ2 (Ped Quaraí 2)	13	02/260	84/009	06/170	0.56 : -0.24 : -0.33 0.99 : 0.19 : 0.10	0.10	25	01/264	87/011	03/174	0.73 : -0.03 : -0.70	0.47	20		
B Pedreira SF Assis 2 (BR377)	20	02/273	72/176	18/003	0.58 : -0.24 : -0.34 0.99 : 0.16 : 0.07	0.10	25	12/275	78/104	02/006	0.71 : 0.03 : -0.73	0.53	25		
C Compilation from sites Estr Velha, Sobradinho1, and Saltinho1A	14	02/174	84/283	06/084	0.24 : 0.12 : -0.36 0.78 : 0.63 : 0.06	0.80	35	08/174	78/305	09/082	0.71 : 0.03 : -0.74	0.53	20		
D Compilation from sites Angico and Poço Grande	17	12/184	76/030	06/275	0.48 : -0.11 : -0.37 0.94 : 0.35 : 0.09	0.30	35	01/190	83/094	07/280	0.73 : -0.01 : -0.73	0.49	35		
E Compilation from sites Sobradinho2, Saltinho2, Gar Zubi, and Pedra Funda	17	02/260	84/152	06/350	0.52 : -0.17 : -0.35 0.97 : 0.27 : 0.10	0.20	30	03/086	87/239	01/356	0.71 : 0.01 : -0.71	0.51	30		
F Compilation from sites Gar Ametista, Pedr Fred Westph, and Caiçara2	20	02/187	72/283	18/096	0.57 : -0.29 : -0.29 0.99 : 0.13 : 0.13	0.00	20	06/187	83/342	03/097	0.73 : -0.03 : -0.71	0.47	20		
G Compilation from sites Pedr Guerra, CODECA1, Aflor Tega, and Veranópolis	11	02/076	84/328	06/166	0.59 : -0.25 : -0.34 1.01 : 0.17 : 0.07	0.10	25	01/072	88/324	02/162	0.79 : -0.02 : -0.77	0.48	30		
H Pedr CODECA1	9	13/184	76/030	06/275	0.50 : -0.12 : -0.38 0.95 : 0.33 : 0.07	0.30	40	02/001	82/105	08/270	0.73 : -0.04 : -0.69	0.46	33		
I Pedreira Painei	10	13/002	76/208	06/094	0.52 : -0.17 : -0.35 0.97 : 0.27 : 0.10	0.20	25	03/008	87/198	01/098	0.72 : 0.01 : -0.72	0.51	39		

7 Results for the linear and multiple-slip methods of inversion are calculated by the T-TECTO 3.0 program, according to Žalohar and Vrabec
8 (2007, 2008).

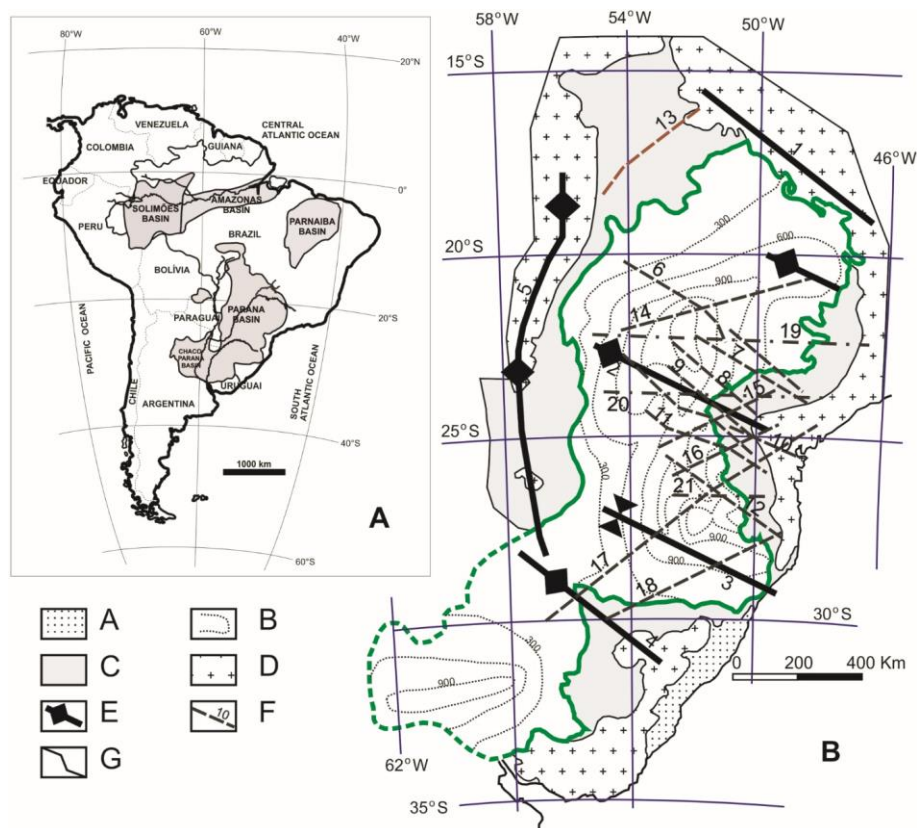
9

10 Table 6 Summary of principal stress axis in the NE–SW orientation computed for sites within the volcanic rocks of the Paraná Basin.

Site	Standard deviation of s	Linear inversion							MSM inversion						
		σ_1	σ_2	σ_3	Relative values of λ_i	D	ϕ_2		σ_1	σ_2	σ_3	Relative values of λ_i	D	ϕ_2	
A Compilation from Pedr Sta Rita 1 + BR293 + Pedr Quarai 1	13	02/027	84/135	06/297	0.62 : -0.27 : -0.36 1.06 : 0.17 : 0.08	0.10	25		02/036	87/165	03/306	0.97 : -0.03 : -0.94	0.48	30	
B Pedreira Sta Rita 2	11	02/309	84/201	06/040	0.65 : -0.27 : -0.37 1.10 : 0.18 : 0.08 0.57 : -0.19 : -0.38	0.10	25		04/113	85/337	04/203	0.82 : 0.01 : -0.83	0.51	35	
C Pedreiras BR290 + BR377	16	02/223	72/320	18/133	1.06 : 0.30 : 0.11 0.51 : -0.12 : -0.40	0.20	25		08/039	80/254	06/130	1.03 : -0.10 : -0.92	0.42	25	
D Compilation from sites Barragem M Filho and Gar Ralph	12	02/236	84/127	06/326	1.01 : 0.38 : 0.10 0.65 : -0.28 : -0.39	0.30	33		07/242	83/058	00/152	0.88 : -0.01 : -0.87	0.49	33	
E Pedreira Dacito	16	13/142	76/296	06/051	1.11 : 0.18 : 0.08 0.57 : -0.19 : -0.38	0.10	30		04/143	72/247	17/052	1.03 : -0.21 : -0.82	0.33	32	
F Compilation from sites Pedreiras FrWestph1, Caiçara1, RodBon1, and Planalto-Alpestre	16	02/125	84/234	06/035	1.05 : 0.29 : 0.10 0.52 : -0.12 : -0.39	0.20	30		04/126	85/273	03/036	0.98 : -0.04 : -0.93	0.47	25	
G Pedreria Rodeio Bonito 2	8	13/058	76/264	06/150	1.01 : 0.37 : 0.10 0.57 : -0.19 : -0.38	0.30	33		15/040	75/230	02/131	0.96 : 0.04 : -1.00	0.53	40	
H Rota dos Canions (RS)	18	02/039	84/148	06/309	1.06 : 0.30 : 0.11 0.52 : -0.12 : -0.39	0.20	30		09/041	81/216	01/310	1.02 : -0.08 : -0.95	0.44	30	
I Compilation from sites Pedreiras BJSerra and Paine12	10	12/212	76/057	06/303	1.01 : 0.37 : 0.10	0.30	35		06/213	84/057	02/303	0.91 : 0.04 : -0.95	0.53	35	

11 Results for the linear and multiple-slip methods of inversion are calculated using the T-TECTO 3.0 program, according to Žalohar and Vrabec
12 (2007, 2008).

13 Figures



24 Abreu–Campo Mourão; 11) Rio Piquiri; 12) Caçador; 13) Transbrasiliano; 14) Araçatuba; 15)
25 Guaxupé; 16) Jacutinga; 17) Lancinha–Cubatão; 18) Blumenau–Soledade; 19) Mogiguaçu–
26 Dourados; 20) São Sebastião; 21) Taquara Verde. G) Main rivers.

27

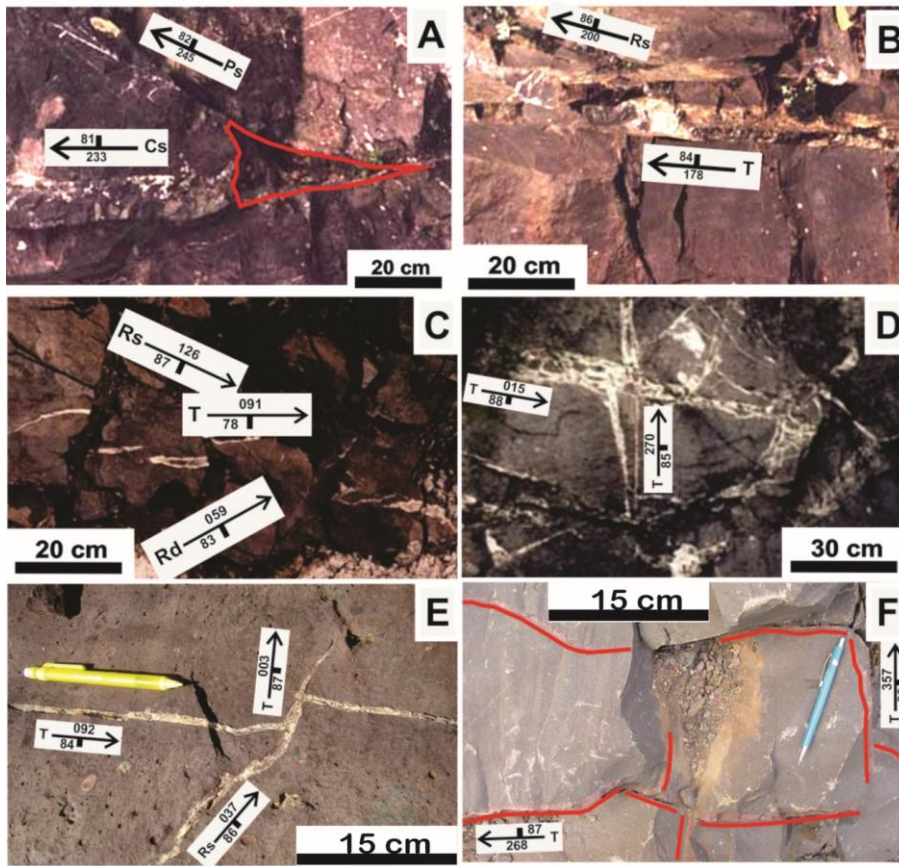
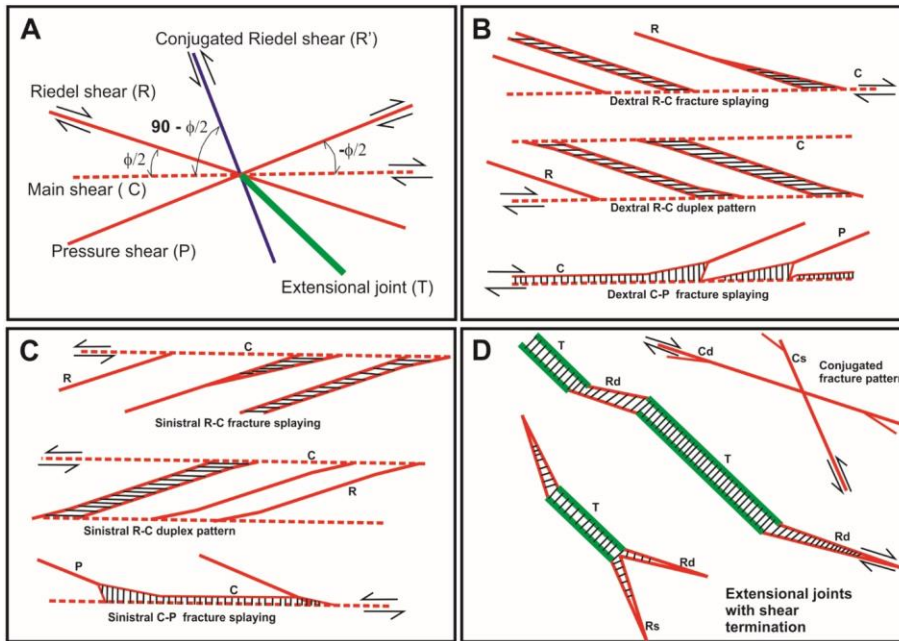


Figure 2 Fracture patterns in the Serra Geral Fm. volcanic rocks. A) Fracture splay and a triangular zone showing hydraulic breccia (weathered). B) Extensional joint terminating into R shear and hydraulic breccia. C) Extensional joints terminating into either dextral or sinistral shear. D) Different generation of extensional joints and hydraulic breccia. E) Orthogonal extensional joints filled by thermally metamorphosed sandstone. F) Orthogonal extensional joints filled by metamorphosed sandstone (the sandstone dykes were laterally delineated). R, C, and P are synthetic shear fractures; R' indicates antithetic shear; T indicates extensional

37 joints; **s** or **d** indicate sinistral or dextral fracture sense of movement, respectively. Notation
 38 for fracture orientation follows Fig. 3.
 39



40
 41 Figure 3 Field diagrams of fracture patterns in the volcanic rocks of the Serra Geral Fm. A)
 42 Riedel-type fractures, as reported by Tchalenko (1970) and Tchalenko and Ambraseys (1970).
 43 B) Dextral patterns of shear fractures. C) Sinistral patterns of shear fractures. D) Conjugated
 44 shear fractures and combinations of tension joints and shear fractures. Hatched areas represent
 45 transtensive dilatational spaces developed by shearing. R, C, and P are synthetic shear
 46 fractures; R' indicates antithetic shear; T indicates extensional joints; **s** or **d** indicate sinistral
 47 or dextral fracture sense of movement, respectively.

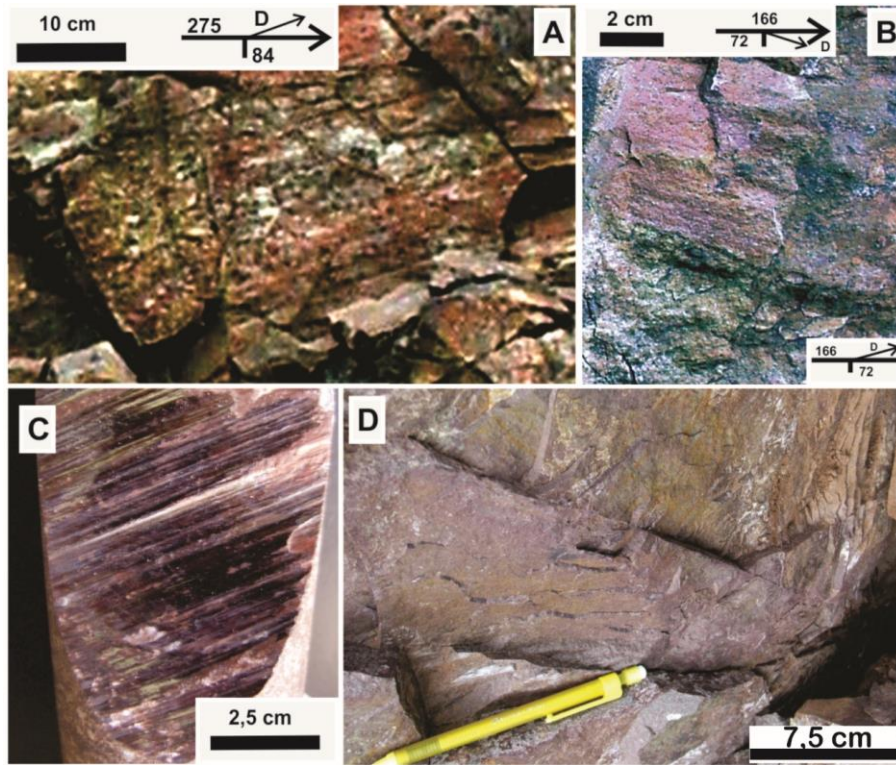
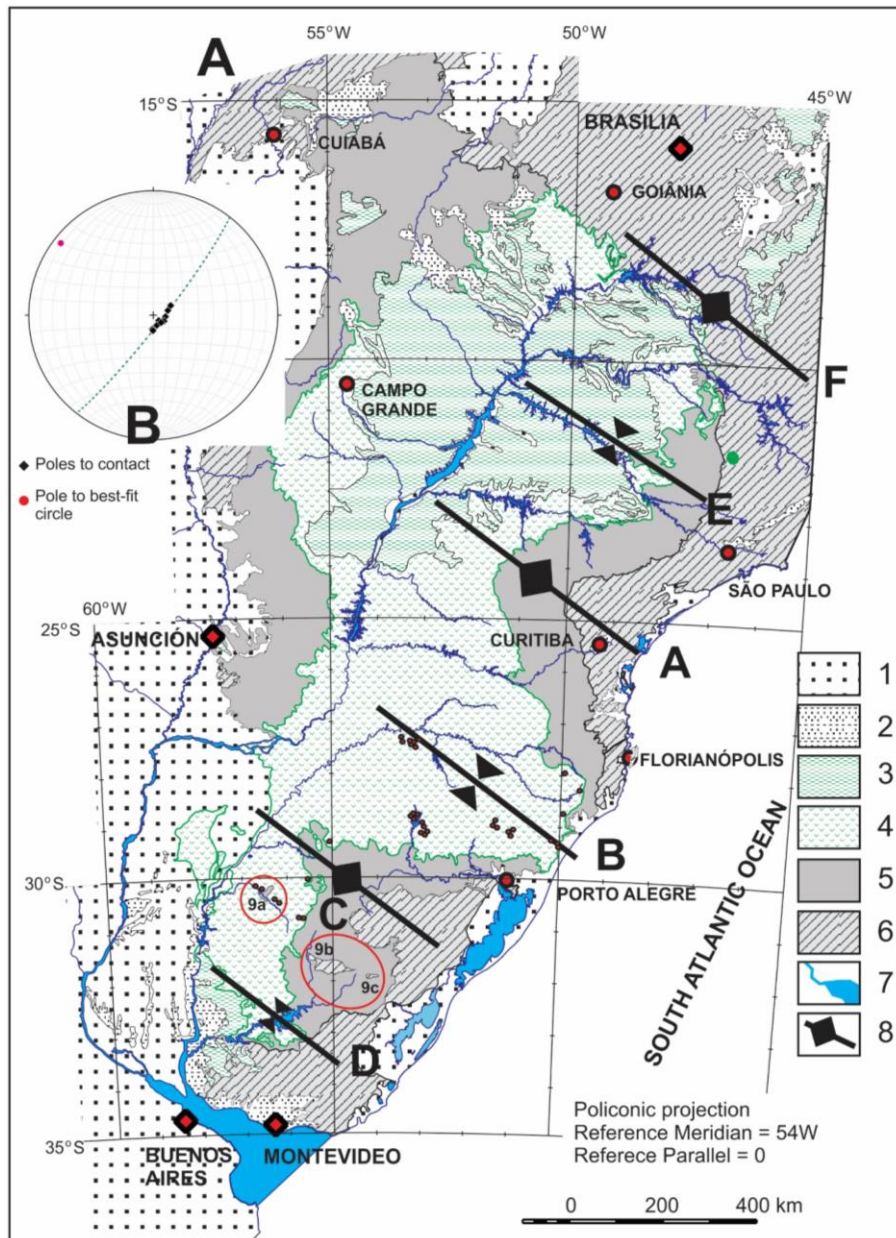


Figure 4 Geological features of the fault planes in the volcanic rocks of the Paraná Basin. A) RM-type striation. B) Overprinting of TM striation on former striation with mineralization in the same fault plane. C) Frictional striae and steps in a polished fault plane. D) Sub-centimeter fracture cleavage dragging the horizontal joints of basalt.



57

58 Figure 5 Regional folds developed by NE-SW paleostress tensors. A) Map showing the

59 location of synclines and anticlines (arcs), and also the domes and basins in the southern part

of the Paraná Basin. B) Lower hemisphere, equal area stereogram of the basal contact of the Serra Geral Fm. along the Rio Grande Arc and Torres Syncline ([dashed line is the best-fit great circle to poles](#)). 1) Quaternary sediments. 2) Cenozoic sedimentary rocks. 3) Cretaceous to Paleogene sedimentary rocks. 4) Paraná Flood Basalts. 5) Paleozoic–Mesozoic sedimentary rocks of Paraná Basin. 6) Basement rocks. 7) Main rivers, lakes, and lagoons. 8) Main NW-oriented arcs and synclines. 9) Elongated domes ([red circles do highlight](#)): a) Quaraí Dome ([see Fig. 7 for a detailed map](#)), b) Rivera Crystalline Island, c) Aceguá Crystalline Island. Based on South America Geological Map (Schobbenhaus and Bellizzia 2001). Small open dots represent outcrops where fault-slip data were measured and analyzed.

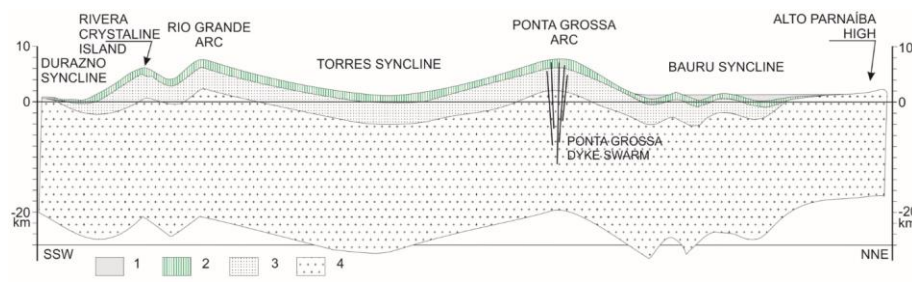
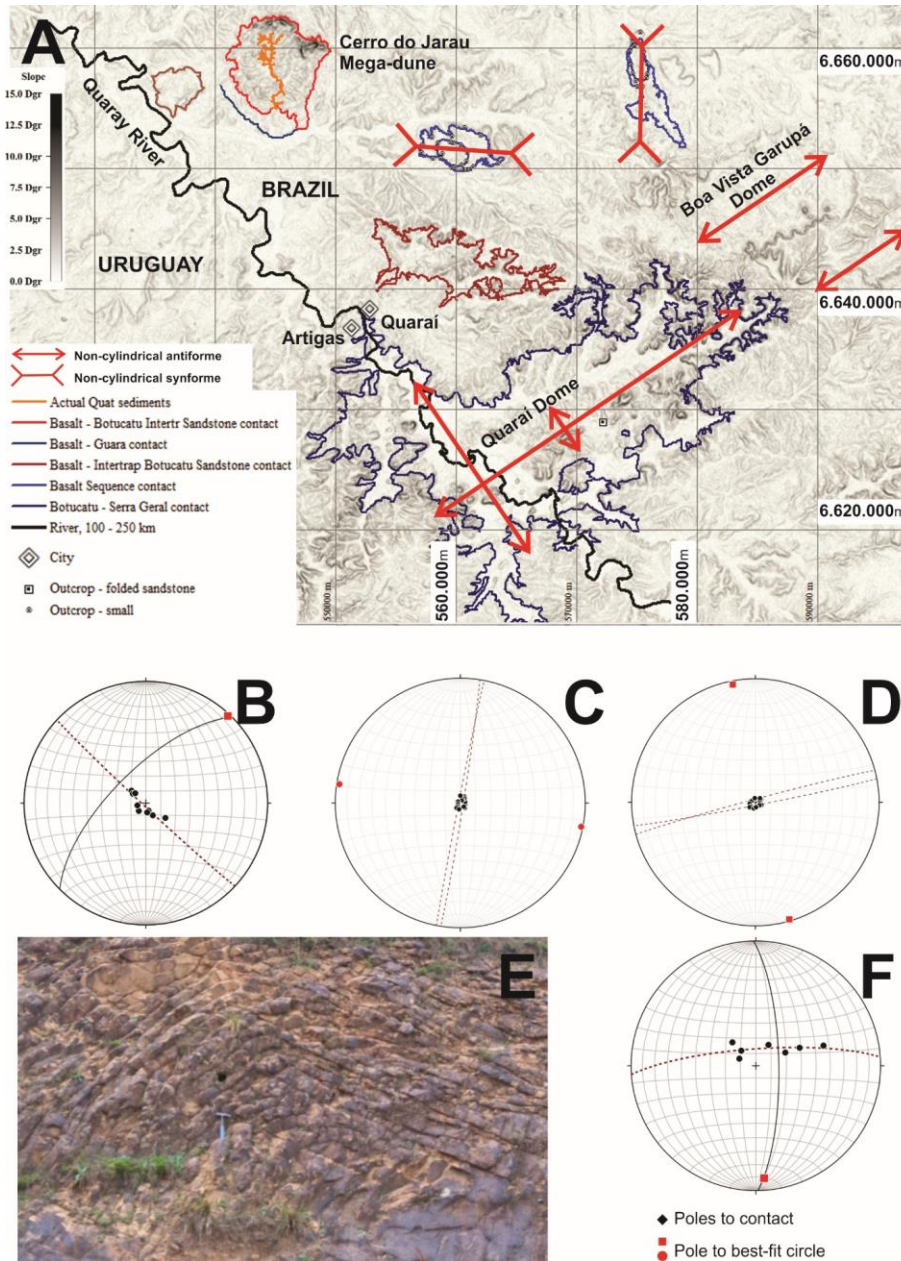


Figure 6 Balanced SW–NE cross section from Uruguay to São Paulo (Brazil) showing the gentle anticlines and synclines dipping NW in the eastern border of the Paraná Basin. The cross section is perpendicular to the fold hinge. 1) Cretaceous to Paleogene sedimentary cover. 2) Serra Geral Fm. 3) Paleozoic–Mesozoic sedimentary rocks of the Paraná Basin. 4) Basement. The structural section was built upon the South America Geological Map (Schobbenhaus and Bellizzia 2001), and structural field data. The vertical exaggeration is 13×.



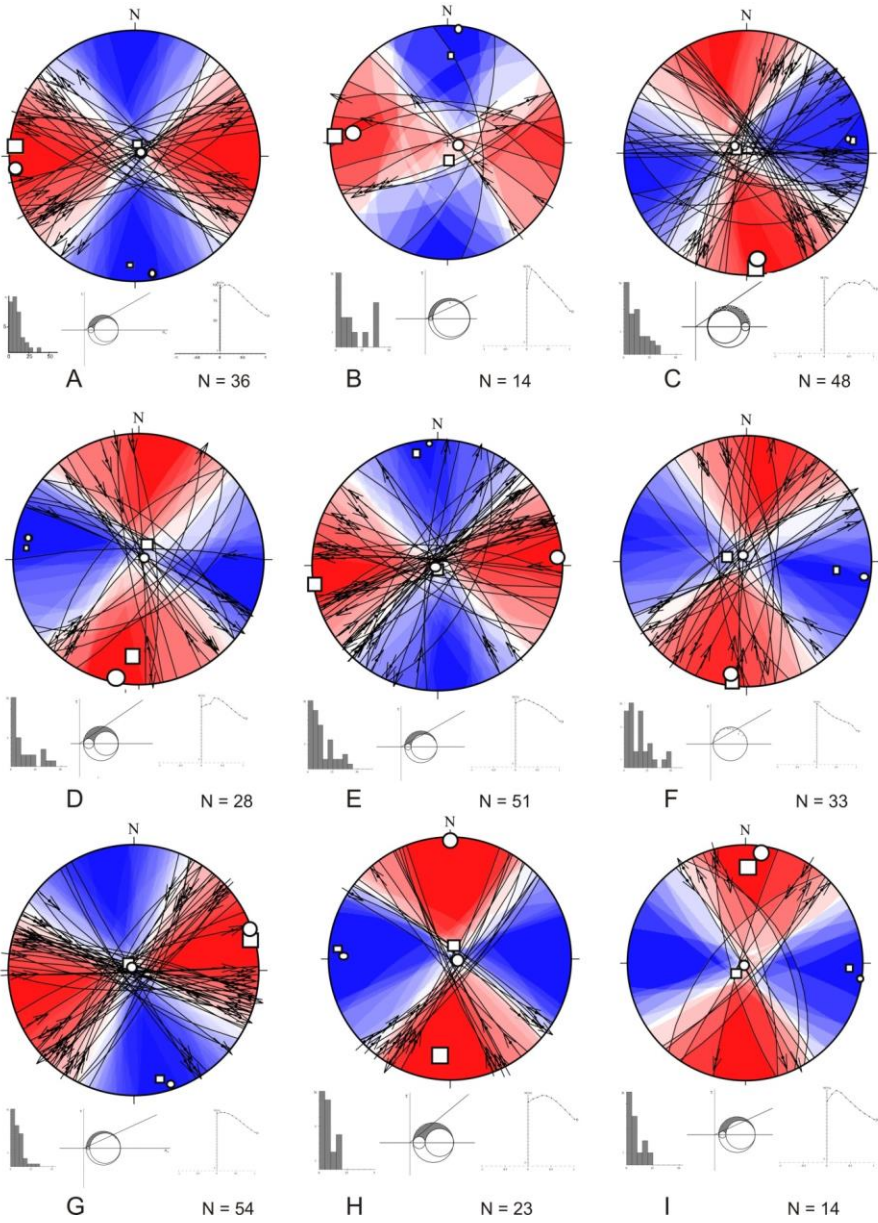
80

81 Figure 7 Dome and basin structures in the Quarai Dome area. A) Geological sketch indicating

82 the main structural features in the region. B) π diagram for sandstone-basalt contact in the

83 Quarai Dome. C) π diagram for a basalt flow contact along the E–W basin. D) π diagram for
84 the basalt flow contact along the N–S basin. E) South-dipping fold in Botucatu Fm.
85 sandstone. F) π diagram for sandstone in the road cut outcrop. [\(Dashed lines in stereograms](#)
86 [are best-fit great circle to poles; continuous lines are axial plane to folds\).](#)

87



89
90 Figure 8 Paleostress results for the N-S and E-W tensors observed in the volcanic rocks of
91 the Paraná Basin. Each area/site is identified by a capital letter. The graphics for each area/site

92 include: lower hemisphere, equal area stereogram of brittle fault-slip data; misfit angle
93 histogram; Mohr diagram for resolved shear stress; and biplot of the value for object function
94 (M) vs. shape of the strain ellipsoid (D). Open circles and open squares in the stereograms
95 represent stress direction determined using the Gauss and MSM methods, respectively. The
96 sizes of the open circles and squares relate to the magnitudes of the stress tensors. [The](#)
97 [stereograms show the fault planes and their respective striae and sense of movement. Red and](#)
98 [blue areas of stereograms represent P and T fields according Angelier and Mechler \(1977\).](#)
99 [respectively.](#)

100

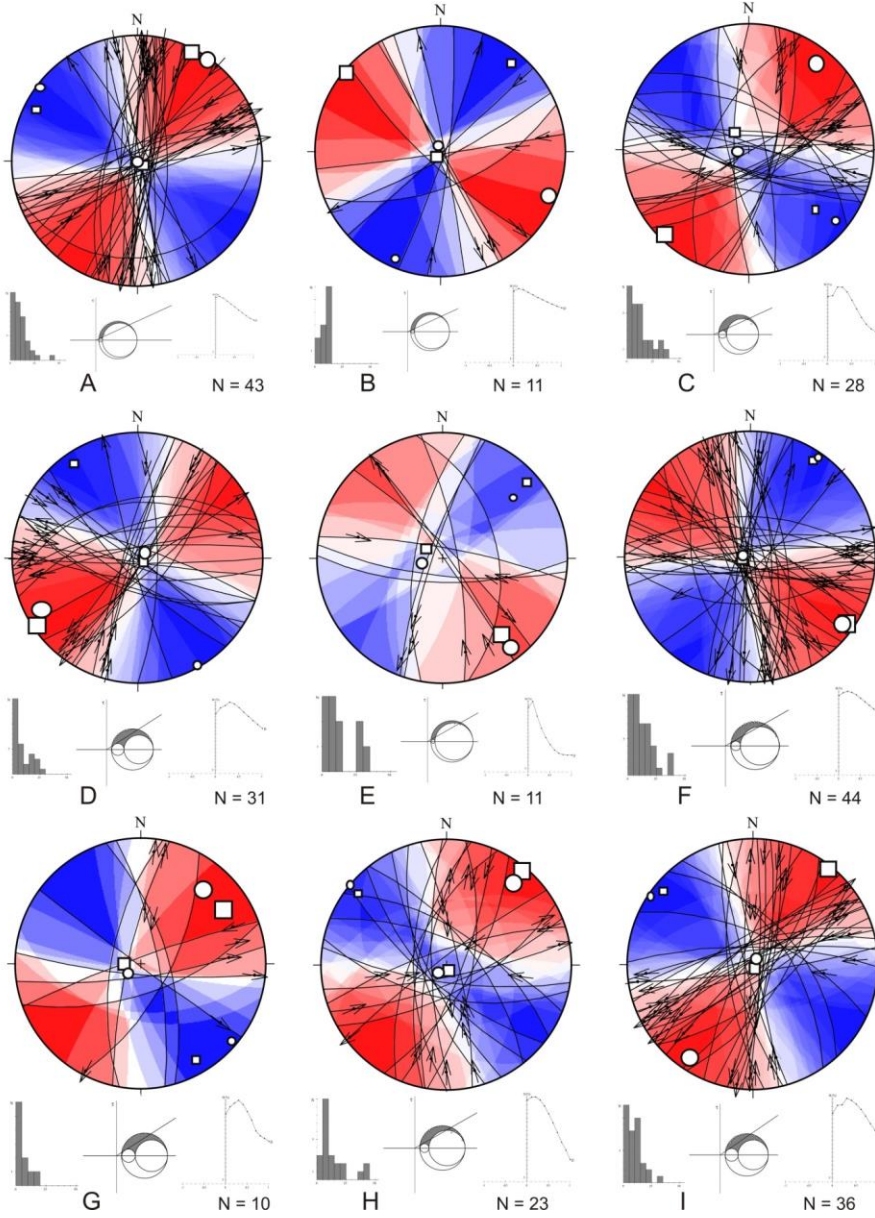


Figure 9 Paleostress results for NE-SW tensors observed in the volcanic rocks of the Paraná Basin. Each area/site is identified by a capital letter. The graphics for each area/site include: lower hemisphere, equal area stereogram of brittle fault-slip data; misfit angle histogram;

105 Mohr diagram for resolved shear stress; biplot of value for object function (M) vs. shape of
 106 the strain ellipsoid (D). Open circles and open squares in the stereograms represent stress
 107 direction determined using the Gauss and MSM methods, respectively. The sizes of the open
 108 circles and squares relate to the magnitudes of the stress tensors. [The stereograms show the](#)
 109 [fault planes and their respective striae and sense of movement. Red and blue areas of](#)
 110 [stereograms represent P and T fields according Angelier and Mechler \(1977\), respectively.](#)
 111

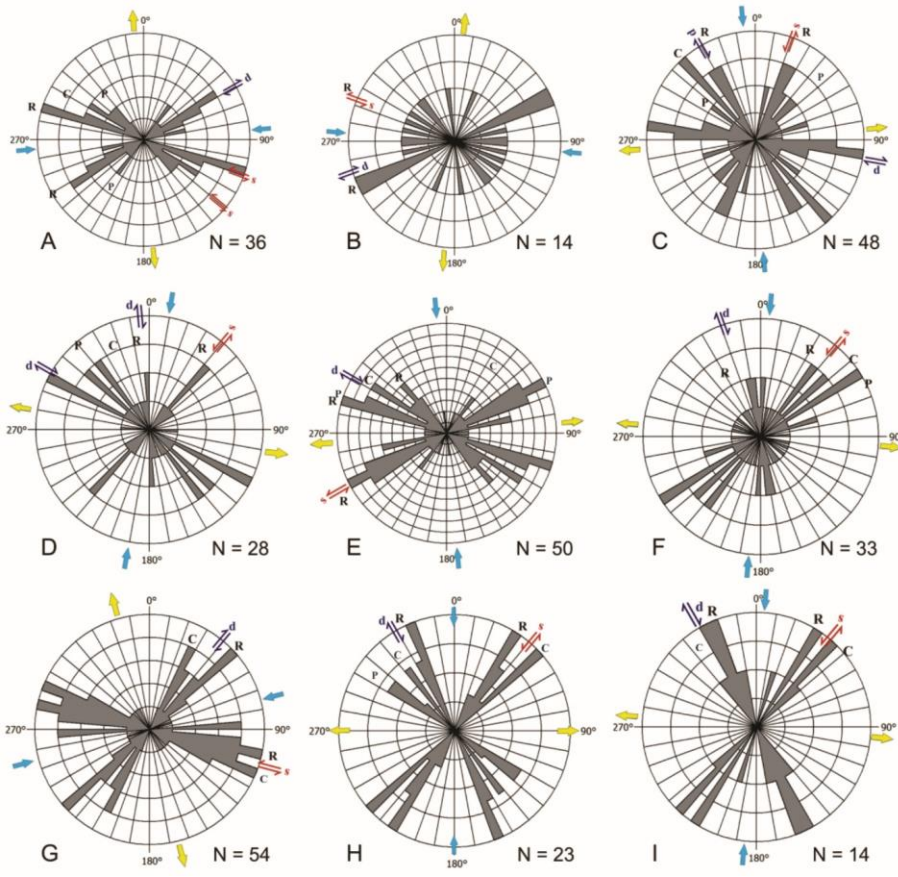


Figure 10 Rose diagrams of fault-slip data for N–S tensors. Circular histograms from A to I correspond to the sites/areas described in Table 3. [Blue and yellow arrows represent maximum and minimum stress tensor orientation from Fig. 8.](#)

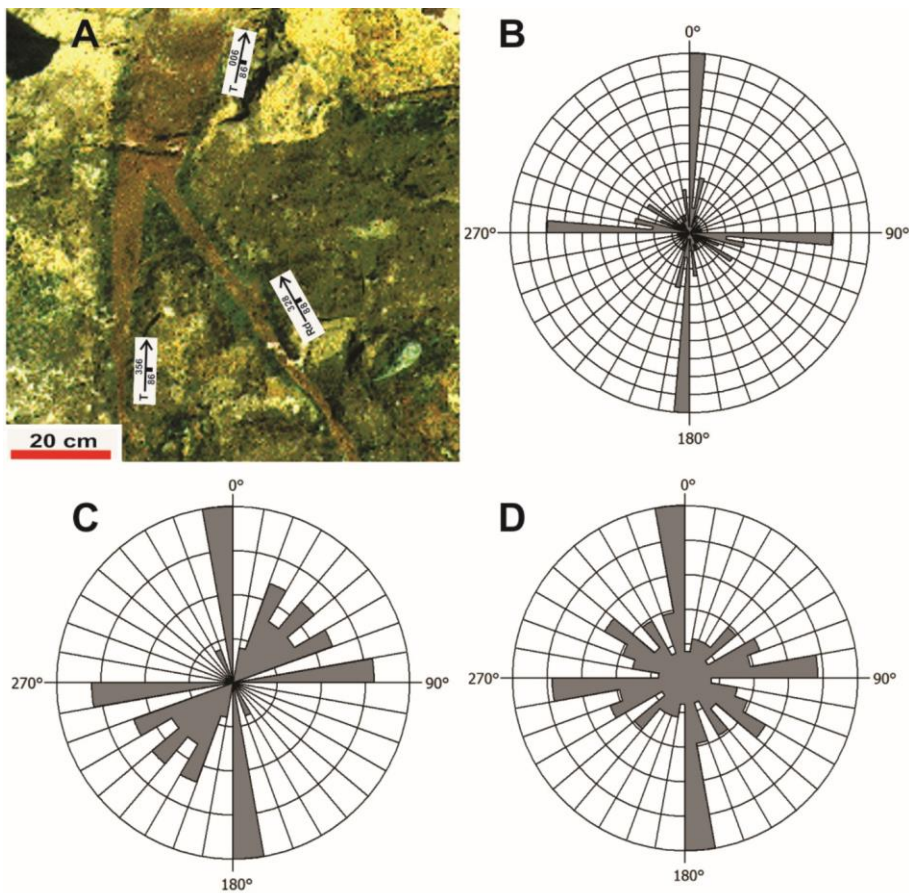


Figure 11 Tabular dykes emplaced into basalts of the Serra Geral Fm. A) Photograph of the tabular dykes emplaced into the vesicular basalts of the Salto do Jacuí region. B) Rose diagram of orientation of sandstone dykes in the Salto do Jacuí region (N = 135). C) Rose

- 122 diagram of orientation of sandstone dykes in the Caxias do Sul region ($N = 24$). D) Rose
- 123 diagram of orientation of mineralized veins in the Caxias do Sul region ($N = 85$).
- 124
- 125

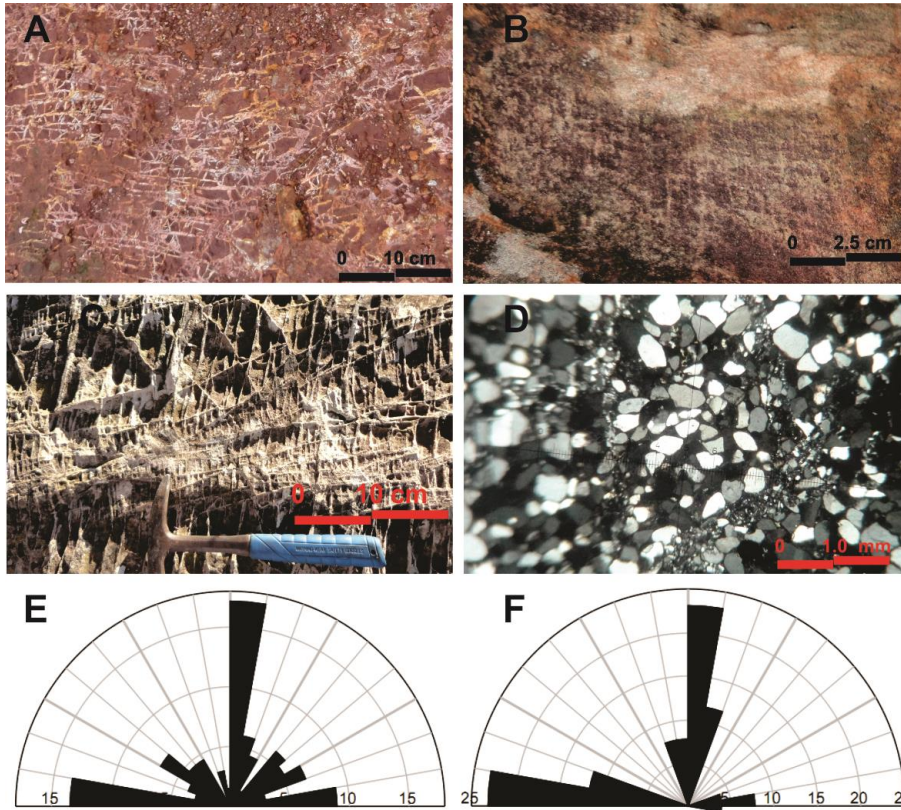


Figure 12 Orthogonal pattern features recorded in the Cerro do Jarau intertrap megadune. A) Centimeter-scale orthogonal “ladder-type” veins in the basalt of the Cerro do Jarau hills. B) Millimeter-scale orthogonal “grid-type” deformation bands in the Botucatu Fm. sandstone in the Cerro do Jarau intertrap dune. C) Superposed shear deformation bands on orthogonal bands. D) Thin section of thermally metamorphosed sandstone showing the orthogonal deformation bands. E) Rose diagram of the orthogonal veins in basalts (N = 134). F) Rose diagram of deformation bands in sandstones (N = 28).

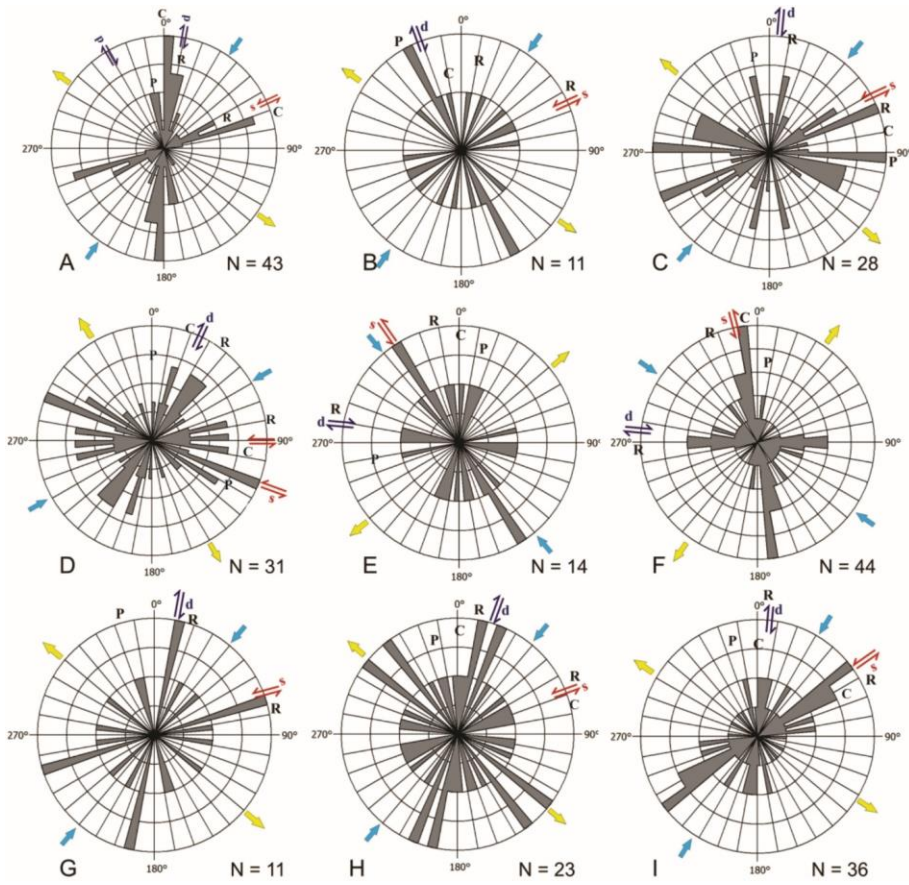


Figure 13 Rose diagrams of fault-slip data for NE-SW tensors. Circular histograms from A to I correspond to sites/areas described in Table 4. [Blue and yellow arrows represent maximum and minimum stress tensor orientation from Fig. 9.](#)

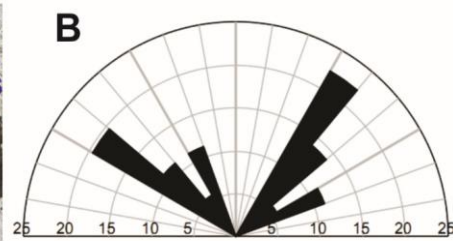


Figure 14 Orthogonal patterns associated with second deformational phase in the Cerro do Jarau area. A) NE-SW orthogonal deformation bands superposed upon the N-S bands. B) Rose diagram of the NE-SW orthogonal deformation bands (N = 36).

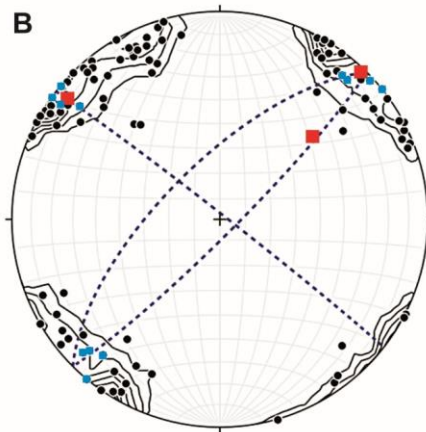
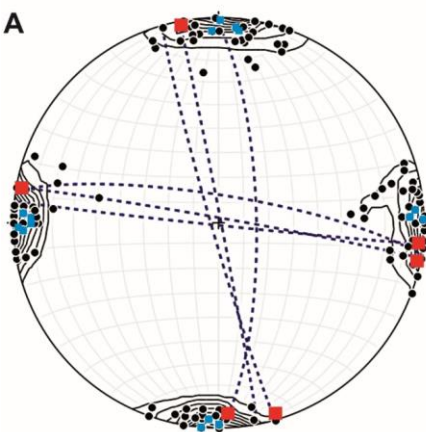


Figure 15 Lower hemisphere stereograms showing the symmetry relationships between domes and basins and fractures in the Paraná Basin volcanics. A) Fold axis (red squares), extensional dykes and veins (blue squares), and deformation bands (black dots) of the first deformational phase in the Quaraí Dome area. B) Fold axis (red squares) for NW regional arcs, Quaraí Dome, extensional dykes and veins (blue squares), and deformation bands (black

dots) of the second deformational phase. Dashed great circles are axial planes of folds and arcs.

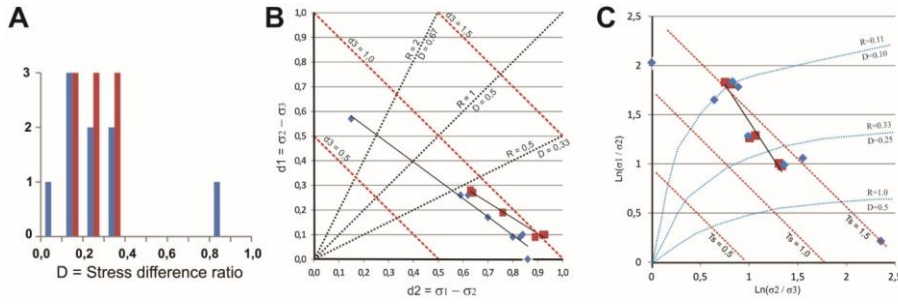


Figure 16 Diagrams for stress states of the deformation phases in the Serra Geral Fm. volcanics, as determined by the linear inversion technique. A) Histogram for D values determined in each investigation area. B) Stress differences diagram of Lisle (1979). C) Stress ratio diagram of Morris and Ferrill (2009). Blue bars and diamonds represent N–S-oriented stress tensors. Red bars and squares represent NE–SW-oriented stress tensors. Thin black lines are the linear best fit for each paleostress regime. $R = d1/d2$ (Lisle 1979). $D = \Phi$ (Angelier 1989). $R = D/(1-D)$.

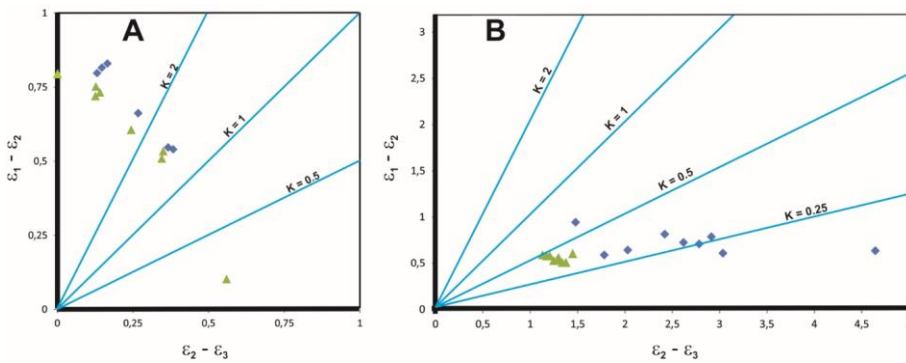
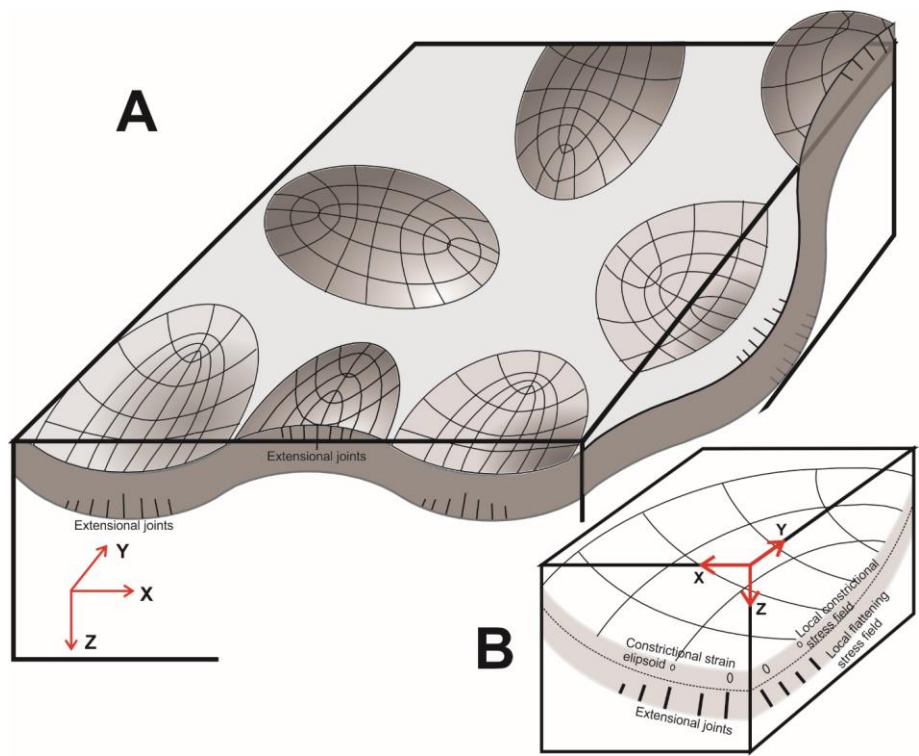


Figure 17 Strain-ratio log diagrams for volcanic rocks of the Paraná Basin. A) Results from the linear inversion method (Žalohar and Vrabec 2007). B) Results from multiple-slip method

167 (Žalohar and Vrabec 2008). Green triangles represent the first deformational phase and blue
 168 diamonds the second.



169
 170 Figure 18 Bi-directional dome-and-basin model structures for the Serra Geral Fm. volcanics
 171 (Paraná Basin). A) Regional sketch for orthogonal elliptical non-cylindrical folds. B) Detail
 172 for local-scale stress/strain distribution in the tangential-longitudinal buckled volcanic layer;
 173 stippled line distinguishes the neutral surface. The principal curvature directions (contour
 174 lines for domes and basins) parallel to the principal strain directions give rise to orthogonal
 175 joints in the outer rims of non-cylindrical folds (Lisle 1999).

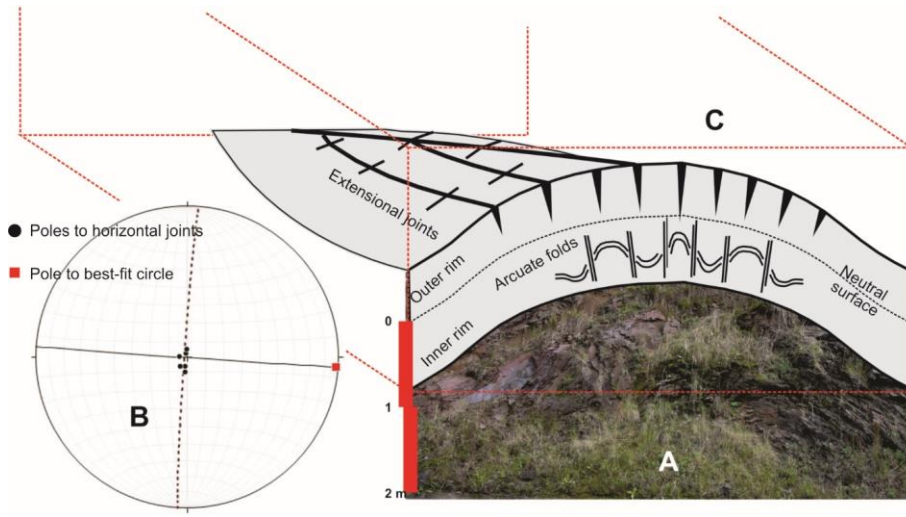


Figure 19 Small-scale fold on basal horizontally jointed basalt flow. A) Outcrop-scale fold at base of a basalt flow. B) Lower hemisphere stereogram for folded horizontal joints of the basalt flow (Dashed lines in stereograms are best-fit great circle to poles; continuous lines are axial plane to folds). C) Tangential-longitudinal buckle model distinguishing structural features developed at the outer and inner rims of a buckled single layer flow.